The very-high resolution configuration of the EC-Earth global model for HighResMIP

Eduardo Moreno-Chamarro[1,2*], Thomas Arsouze[1,3], Mario Acosta[1], Pierre-Antoine Bretonnière[1], Miguel Castrillo[1], Eric Ferrer[1], Amanda Frigola[1], Daria Kuznetsova[1], Eneko Martin-Martinez[1], Pablo Ortega[1], Sergi Palomas[1]

1. Barcelona Supercomputing Center (BSC), Barcelona, Spain
2. Now at: Max Planck Institute for Meteorology, Hamburg, Germany
3. Now at: CIRAD, UMR AMAP, F-34398 Montpellier, France
* Corresponding author: eduardo.chamarro@mpimet.mpg.de

Abstract

We here present the very-high resolution version of the EC-Earth global climate model, EC-Earth3P-VHR, developed for HighResMIP. The model features an atmospheric resolution of ~16 km and an oceanic resolution of 1/12° (~8 km), which makes it one of the finest combined resolutions ever used to complete historical and scenario-like CMIP6 simulations. To evaluate the influence of numerical resolution on the simulated climate, EC-Earth3P-VHR is compared with two configurations of the same model at lower resolution: the ~100-km-grid EC-Earth3P-LR, and the ~25-km-grid EC-Earth3P-HR. Out of the three configurations, VHR shows the smallest drift in the global mean ocean temperature and salinity at the end of a 100-year 1950's control simulation, which points to a faster equilibrating phase than in LR and HR. In terms of model biases, we compare the historical simulations ~~The models' biases are evaluated~~ against observations over the period 1980–2014. In contrast~~Compared~~ to LR and HR, VHR shows a reduced equatorial Pacific cold tongue bias, an improved Gulf Stream representation, with a reduced coastal warm bias and a reduced subpolar North Atlantic cold bias, and more realistic orographic precipitation over mountain ranges. By contrast, VHR shows a larger warm bias and overly low sea ice extent over the Southern Ocean. Such biases in surface temperature have an impact on the atmospheric circulation aloft, connected with more realistic~~with improved~~ stormtrack over the North Atlantic, yet less realistic~~worsened~~ stormtrack over the Southern Ocean compared to the lower resolution model versions. Other biases persist or worsen with increased resolution from LR to VHR, such as the warm bias over the tropical upwelling region and the associated cloud cover underestimation, a~~and the~~ precipitation excess over the tropical South Atlantic and North Pacific, and an overly thick sea ice and an excess in oceanic mixing in the Arctic. VHR shows improved air–sea coupling over the tropical region, although it tends to overestimate the oceanic influence on the atmospheric variability at mid-latitudes compared to observations and LR and HR. Together, these results highlight the potential for improved simulated climate in key regions, such as the Gulf Stream and the Equator, when the atmospheric and oceanic resolutions are finer than 25 km in both the ocean and atmosphere. Thanks to its unprecedented resolution, EC-Earth3P-VHR offers a new opportunity to study climate variability and change of such areas on regional/local spatial scales, in line with regional climate models.

 2

1. Introduction

Interest in high-resolution modeling has soared in the past years, specially thanks to large European research projects and initiatives such as PRIMAVERA (PRIMAVERA and the European Commission, 2015), nextGEMS (Hohenegger et al., 2023, Rackow et al., 2024), EERIE, and Destination Earth (Hoffmann et al., 2023) (last access: 20 June 2024). Broadly, these projects seek to build the next generation of high-resolution global climate (or Earth system) models capable of representing climate phenomena with unprecedented accuracy, to simulate and predict regional climate, guide policymaking, and provide relevant climate information to end users. Thanks to these efforts, high-resolution models at resolutions of 25–50 km or even finer have been provenproved to lead to reduced biases in the simulated climate (see Introduction in Moreno-Chamarro et al., 2022 for a review), and to a better representation of, for example, tropical cyclones (Roberts et al., 2020a; Vidale et al., 2021; Zhang et al., 2021), storm-tracks (e.g., Hodges et al., 2011), the intertropical convergence zone (ITCZ; e.g., Doi et al., 2012; Tian et al., 2020), or the Gulf Stream and associated air–sea interactions (e.g., Kirtman et al., 2012; Bellucci et al., 2021) compared to standard resolution models (hereafter, ~100-km grid). An extensive review of the benefit of high-resolution modeling can be found in Haarsma et al. (2016), Hewitt et al. (2017), Roberts M.J. et al. (2018), and Czaja et al. (2019). However, increased model resolution alone is not always the answer: for example, persistent, well-known biases in clouds and radiation can be insensitive to an increase in atmospheric resolution from a ~100-km grid to a 25–50-km grid (Moreno-Chamarro et al., 2022). Inadequate model physics or insufficient tuning can thus mask or negate the benefits of increased resolution.

High-resolution modeling faces additional challenges. One is the high computational cost of running the simulations, and another, related, is the difficulty of achieving high throughput due to the loss of efficiency with increasing parallelization.~~One is the large computational cost needed to complete the simulations, which also limits the model throughput.~~ These~~Both~~ issues have gradually improved thanks to steady increases in supercomputing power and parallel enhancements in model efficiency to leverage that power. The community trusts in High Performance Computing (HPC) to increase the performance of climate models, developing different approaches to speed models up. These approaches can go from improving the traditional parallelization algorithms (Tintó Prims et al., 2019a) or reducing the accuracy of the variables from double to single precision (Váňa et al., 2017, Tintó Prims et al., 2019b) to

3

increasing the Input/Output throughput of complex model configurations (Xepes-Arbós et al., 2022, Sarmany et al., 2024). Faster models are also needed to complete, in a reasonable time, the tuning and the spin-up phases, which for a high-resolution model, can be extremely costly. The demand for high efficiency in high-resolution modeling has therefore accelerated the development and implementation of new modeling strategies to ensure an optimal use of the computing resources.

High-resolution models also need to find a fair compromise between the resolutions of the different climate components, which, sometimes, can be very disparate—for example, an eddy-rich ocean model (~10 km grid) coupled to a 25 km, 50 km, or even coarser-grid atmosphere model (e.g., Gutjahr et al., 2019, Rackow et al., 2019, Semmler et al., 2020). Tsartsali et al. (2022), for example, reported increased ocean–atmosphere coupling strength and better agreement with reanalysis and observations over the Gulf Stream, when both the ocean and atmosphere resolutions are increased to comparable ~25-km grid at least. Moreton et al. (2021) showed a degraded representation of the air–sea interaction at increased oceanic resolution but a constant atmospheric resolution. Similarly, Ma et al. (2016) found that the mesoscale ocean temperature affects the storm track over the Pacific only when the atmospheric model resolution is enough to resolve the small-scale diabatic heating. Finally, Rai et al. (2023) described a disproportionate eddy killing when a coarse 200-km wind forcing is used to force a finer (~10–25-km) ocean, compared to the case with similar grid sizes. These results of these studies thus advocate for a similar resolution in both the atmosphere and ocean.

Sometimes, ~~H~~high-resolution modeling ~~usually~~ relies on single-model component, either atmospheric-only (Baker et al., 2019) or ocean-only configurations (e.g., Biastoch et al., 2021), or on regional models (e.g., Woollings et al., 2010; Ma et al., 2017) as in CORDEX (Jacob et al., 2014) for hypothesis testing and downscaling climate projections. Such configurations, however, lack global energy constraints, remote influences, and, potentially, key feedbacks rectifying the mean state. These models are also limited by the boundary conditions, which often are derived from coarser (~100 km) global models and can present biases in their mean climate that might be absent or much reduced at a higher resolution; these biases might then be passed onto the single model configurations. For example, an overly smooth Gulf Stream temperature gradient, an incorrect separation, or the lack of mesoscale in ocean temperatures can impact the response of the atmospheric circulation aloft (e.g., Ma et al., 2017; Lee et al., 2018). Low-resolution and

4

high-resolution global models can also respond differently to climate change: for example, the northward shift and strong surface warming of the Gulf Stream projected by the eddy-rich configuration of the HadGEM3-GC3.1 model for the 21st century is absent at the lower-resolution model versions (Moreno-Chamarro et al., 2021). Associated with this, the increase in winter precipitation is similarly much larger over Europe at the highest resolution than at any lower one, which reinforces the idea that the response of the atmosphere is strongly sensitive to the boundary conditions. These findings put a limit to our confidence in single-model configurations and regional models, since they lack a global dynamical response.

As a response to the listed challenges, we here present the eddy-rich version of the EC-Earth climate model for PRIMAVERA/HighResMIP. This is likely one of the finest combined horizontal resolution global models ever used to complete CMIP-like simulations, with a nominal resolution of about 10–15 km; it also has the additional advantage that the resolution is comparable in both the atmosphere and ocean/sea-ice, which allows the atmosphere to “see” the fine-scale forcing from the ocean with minimal information lost from interpolation. In this paper, we describe the model configuration and the developments in model efficiency (Section 2), as well as the main characteristics of its climate for the period 1980–2014 compared to observations (Section 3).

2. Model Description and Experimental Setup

2.1 Model description

All HighResMIP contributions with the EC-Earth global coupled climate model have been performed with its version 3.2.2, developed within the PRIMAVERA project (EC-Earth3P). The model consists of ~~the~~ atmosphere, ocean, and sea ice components. The atmosphere model is based on the ECMWF Integrated Forecasting System (IFS), in the 36r4 cycle (based on IFS system 4, https://www.ecmwf.int/sites/default/files/elibrary/2011/11209-new-ecmwf-seasonal-forecast-system-system-4.pdf, last access: 8 November 2024). A detailed account of the changes introduced in this cycle can be found on the ECMWF website (https://confluence.ecmwf.int/display/FCST/Implementation+of+IFS+Cycle+36r4, last access: 20 June 2024). The very-high resolution version of the model, EC-Earth3P-VHR, features a triangular truncation at wave number 1279 (hence known as T1279) in spectral space, with a linear N640 reduced Gaussian grid. This corresponds to a spacing of ~16 km. However, because

5

of the complexity of numerical solutions and parametrizations, the effective resolution (this is the smallest scale IFS T1279 can fully resolve) is of ~120 km (Abdalla et al., 2013). Vertically, the model features 91 levels, resolving the middle atmosphere up to 0.01 hPa. The model time step during the simulation was 360 s. IFS integrates the revised land surface hydrology Tiled ECMWF Scheme for Surface Exchanges over Land (H-Tessel) model (Balsamo et al., 2009; Hazeleger et al., 2012).

The ocean model is the Nucleus for European Modelling of the Ocean in its version 3.6 (NEMO3.6; Madec, 2008, Madec and the NEMO team, 2016). This is a hydrostatic, finite-difference, free-surface, primitive equation general circulation model. EC-Earth3P-VHR uses the ORCA12 tripolar grid, with the horizontal resolution increasing from the Equator to the poles: ~9 km at the Equator, ~7 km at mid-latitudes, and ~2 km near the poles. This corresponds to an effective resolution of ~45 km (roughly five times the ORCA grid spacing; Soufflet et al., 2016). The model uses a z* coordinate system for the vertical grid and has 75 vertical levels, with the resolution decreasing from 1 m at the surface to 200 m in the deep ocean. The bottom topography is derived from the combination of ETOPO1 (Amante and Eakins, 2009) and GEBCO_08 (Becker et al., 2009). VHR does not include an ocean current feedback (Renault et al., 2023). The sea ice model is the Louvain-la-Neuve sea Ice Model in its version 3 (LIM3) (Vancoppenolle et al., 2012). This is a dynamic-thermodynamic sea ice model, with five ice thickness categories. The time steps are 240 s for NEMO3.6, and 720 s for LIM3 in the EC-Earth3P-VHR.

The atmosphere–land and ocean–sea-ice components are coupled through the OASIS (Ocean, Atmosphere, Sea Ice, Soil) coupler, version 3 (OASIS-MCT 3.0) (Valcke and Morel, 2006; Craig et al., 2017). OASIS remaps the atmosphere fluxes onto the ocean grid via nearest-neighbor distance-based Gauss-weighted interpolation. The exchange includes the transfer of momentum, energy, and mass fluxes from the atmosphere to the ocean, while sea-surface temperature and sea ice and snow variables from the ocean to the atmosphere. The remapping of runoff from the atmospheric grid points to runoff areas on the ocean grid was re-implemented to be independent of the grid resolution. This was done by introducing an auxiliary model component and relying on the interpolation routines provided by the OASIS coupler. More details on the coupling are provided by Döscher et al. (2022).

6

EC-Earth3P-VHR (hereafter, VHR) is compared with two lower-resolution global model versions, also run within the PRIMAVERA/HighResMIP project: EC-Earth3P (hereafter, LR; EC-Earth Consortium, 2019), and EC-Earth3P-HR (hereafter, HR; EC-Earth Consortium, 2018). In the atmosphere, they use the T255 (~107 km) and T511 (~54.2 km) spectral resolution of the IFS model respectively (equivalent to an effective resolution of ~600 km and ~280 km respectively; Abdalla et al., 2013), both with 91 vertical levels. In the ocean, LR and HR use the ORCA1 (~100 km) and ORCA025 (~25 km) tripolar grid respectively (equivalent to an effective resolution of ~500 km and ~125 km respectively; Soufflet et al., 2016), both with 75 vertical levels. They both use the LIM3 sea ice model and the OASIS coupler as well. LR and HR's time steps are respectively 2700 s and 900 s in all the atmosphere, ocean, and sea ice. More details of these two other model versions can be found in Haarsma et al. (2020).

Following the CMIP6 HighResMIP protocol, no additional tuning is applied across resolutions but for a short list of parameters that explicitly change with resolution, particularly for oceanic diffusion and viscosity. The higher resolution in the atmosphere results in a better representation of features such as tropical storms, land/sea transitions, heavy rainfall, and fronts (see Fig. 1 as an example), while in the ocean the increase in resolution allows mesoscale processes to be resolved at a much larger range of latitudes and the representation of finer resolution bathymetric features and coastlines.

2.2 Configuration and workflow setup and performance optimization

The development and maintenance of the EC-Earth model is supported by the EC-Earth Consortium, which shares model code, configurations, and minimal software infrastructure to operate it. While the LR and HR configurations of EC-Earth-3P were developed in a broad collaboration of all the consortium members participating in PRIMAVERA, VHR's development was primarily completed at the Barcelona Supercomputing Center, in collaboration with the Swedish Meteorological and Hydrological Institute (SMHI) within the ESiWACE2 H2020 project (last access: 20 June 2024). The development was conducted on two different supercomputing machines: MareNostrum3, and MareNostrum4 (last access: 20 June 2024). VHR's configuration, at the time of the project, represented one of the most cutting-edge versions of a climate model to run over long time scales. Obtaining a production version of the model, however, entailed ~~the~~ i) generating new grid files; ii) deploying the initial data; iii) generating the coupling weights (see below); iv) creating a new namelist for the ocean NEMO model; v) modifying the runscripts to handle the new files and new configuration; vi) bringing changes from modern versions of the model workflow (Auto-EC-Earth), which, for example, automatizes the call of ELPiN (Tintó et al., 2017; Haarsma et al., 2020) and lets the user fine-tune the distribution of the computational resources in parallel systems; vii) updating the XIOS (the library for input/output management; https://forge.ipsl.jussieu.fr/ioserver, last access: 30 October 2024) to deal with the land suppression; and viii) exploring and modifying the configuration parameters to improve the computational throughput of the model execution without losing result accuracy (see below). ~~development of novel source code and execution scripts, the generation of all requisite files for initializing the simulations, and the adaptation of the model workflow software.~~ This presented a significant challenge for both the operations department and the workflow developers, which were required to fine-tune the system to achieve stable runs and minimize the loss of computing hours. Moreover~~For example~~, generating the interpolation weight files to couple the new model grids for the OASIS coupler was particularly challenging. This process could not readily be parallelized at that time in VHR's OASIS3-MCT coupler version (in contrast to more recent ones), and it required collaborating with the OASIS development group. For the workflow, a significant proportion of the effort was devoted to exploiting the hybrid architecture and integrating the dedicated data transfer nodes available in the MareNostrum4 cluster into the workflow software. Additionally, the automatic algorithm that enables the suppression of land grid subdomains in the NEMO ocean model (ELPiN; Tintó et al., 2017) was incorporated, resulting in a reduction of about 12% in the required HPC resources (see Haarsma et al., 2020 for more details). Finally, the MareNostrum4 new network (100Gb Intel Omni-Path Full-Fat Tree), despite its fast and responsive nature, proved to be quite unstable when subjected to high workloads involving multiple concurrent communications, as was the case of the VHR configuration. However, despite the significant challenges, a~~A~~t the end of the ESiWACE2 project (December 2022), the configuration was ready and all the code was versioned and shared with the other partners within the EC-Earth Consortium.

8

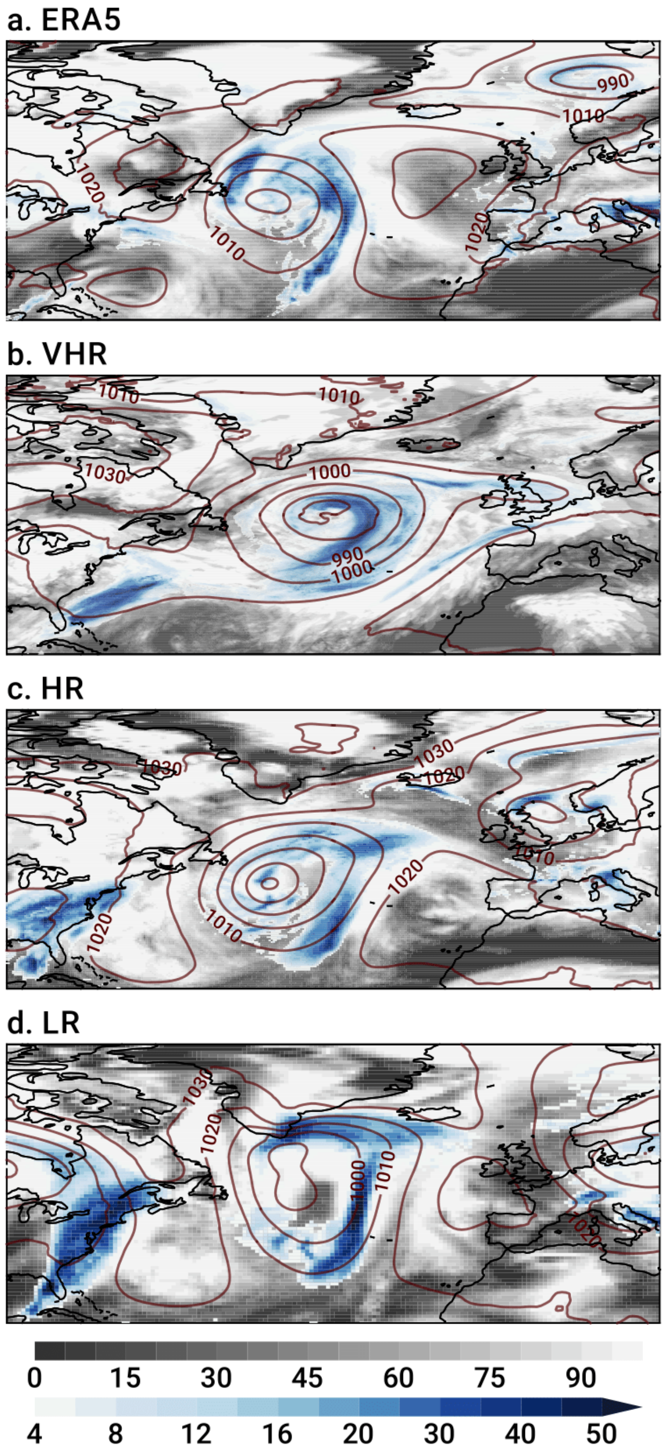

Figure 1. Snapshot of an extratropical storm over the North Atlantic in the winter 1999–2000 in a) ERA5, and in the b) VHR, c) HR, and d) LR models on their original grids. Shown are daily precipitation rate (mmd^{-1}; blue shading), cloud cover (% of area; gray shading), and sea-level pressure (hPa; contours).

9

Once deployed, the workflow needed to be made more efficient to be put into operation. Emerging advancements in global climate modeling demand heightened focus on HPC, particularly to accommodate the increasing need for enhanced model resolution (Acosta et al., 2024). An example of such demanding requirements is the VHR configuration, underscoring the need for efficient resource use. In order to address this issue, we conducted a two-fold HPC performance exercise, which involved both a pure computational performance analysis and a scalability study for each model component (IFS and NEMO), complemented with a load balance optimization for the coupling. This analysis concluded that the coupling and output process could be a bottleneck. An optimization was included to package different coupling fields to be sent in the same MPI (Message Passing Interface) communications, reducing the latency and taking advantage of the bandwidth. Additionally, the I/O (Input/Output) setup was optimized to ensure minimal time was needed to produce the outputs.

While the primary objective of the scalability and load-balance study was to assess the model's efficiency and determine an optimal resource utilization, findings by Acosta et al. (2023) also indicate that enhancing the performance of one component, such as reducing the execution time of IFS, may not necessarily decrease the overall execution time of the coupled model. This discrepancy could stem from a synchronization point at the end of each coupled time step, where both components exchange fields. In cases where other non-optimized components lag behind, a load rebalance becomes necessary.

Concerning the scalability exercise, w~~W~~e ran a series of ~~scalability~~ tests to balance the resources (computing cores) of the VHR's IFS and NEMO models (Fig. 2). To find the most balanced configuration for a given amount of resources, we followed two different but complementary approaches. The first and most costly one tried to find the optimal distribution by assigning the same number of processors to IFS and NEMO first, and moving resources between them alternately; this allowed identifying the intervals for which the model performance increases by using variations of half-interval search algorithm. The second approach to balance the configuration started from one separate scalability test for each model component that was later used to determine the optimal configuration.

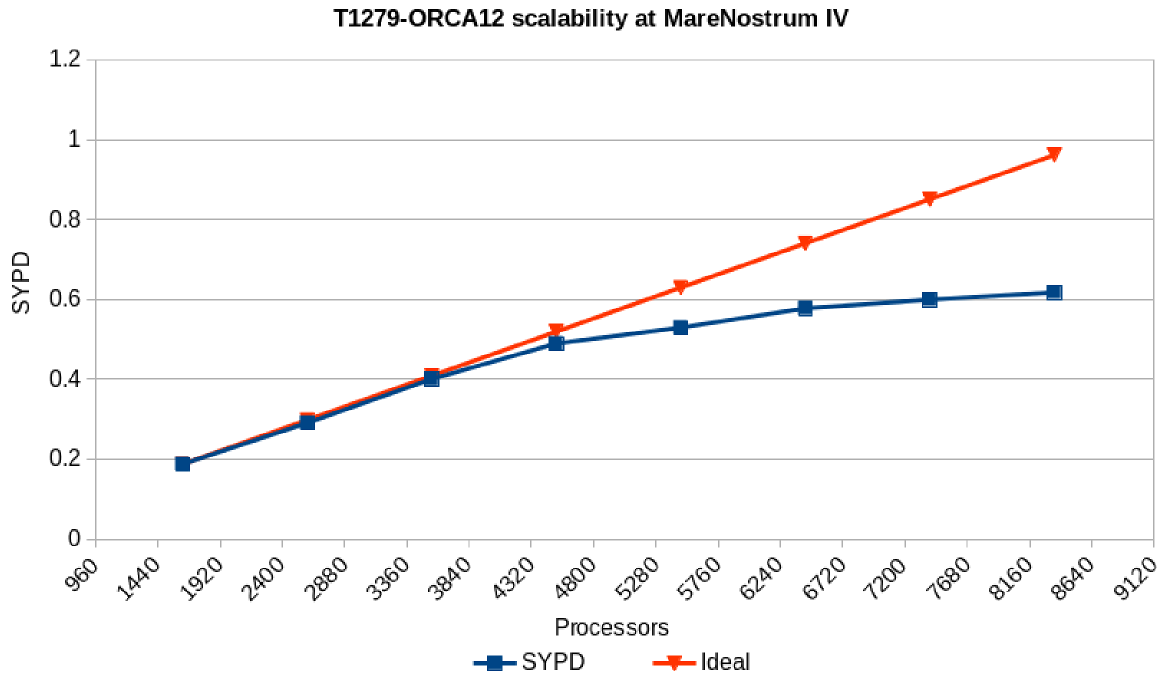

Figure 2. Results of the scalability test of the VHR configuration (T1279 IFS and ORCA12 NEMO) at MareNostrum4 (blue line) in simulated years per day (SYPD) for a given amount of processors. The orange line shows the ideal case with no loss in computing performance.

The workflow software Auto-EC-Earth and, by extension, the simulations described here were configured and run with the workflow manager Autosubmit (Manubens-Gil et al., 2016). This Python package~~toolbox~~ facilitates the production of numerical experiments, like the EC-Earth ones, and it allows easily handling experiments with different members, start dates, and initial conditions. ~~.~~The workflow is~~It creates~~ an oriented graph~~, taking into account every step of the workflow,~~ that includes pre- and post-processing data, the transfer to storage spaces, or the conversion of the output data to CMOR standard, with details on computing resources needed for each step.~~ Autosubmit also allows easily handling experiments with different members, start dates, and initial conditions.~~

2.3 Simulations

The VHR simulations follow the HighResMIP experimental protocol (Haarsma et al., 2016) and consist of: i) a 50-year spin-up run (spin-up-1950), with initial conditions of temperature and salinity from an ocean state representative of the 1950s (Good et al., 2013, EN4 data set) and forcing consisting of well-mixed greenhouse gases, including O_3 and aerosol loading for a 1950s (~10-year mean) climatology; ii) a 105-year control run (control-1950), starting from the end of spin-up-1950 and keeping the same fixed forcing; iii) the historical run (hist-1950), starting from the same initial state as the control, but with time-varying external forcing for the period 1950–2014; iv) and the future scenario run (highres-future), as a continuation of the historical simulation under the CMIP6 SSP5-8.5 scenario (Kriegler et al., 2017) for the period 2015–2050. In this work, VHR's hist-1950 simulation is compared with corresponding hist-1950 runs from LR and HR (Haarsma et al., 2020).

During the model setup, we erroneously applied the EN4 initial conditions at the beginning of all the spin-up runs. While EN4 uses practical salinity and potential temperature, the NEMO model, which uses the TEOS-10 equation of state, requires absolute salinity and conservative temperature. Nonetheless, the differences between the two temperature and salinity types is indeed small (Pawlowicz, 2013; McDougall et al., 2021), and we expect the error to minimize throughout the spin-up (see Section 3.1).

2.4 Observations and reanalysis

As we mainly aim to evaluate the performance of EC-Earth3P-VHR configuration and describe the main model biases and characteristics, we focus on the best-observed part of the historical period of the historical simulations, between 1980 and 2014. The three model configurations are compared with the following observational and reanalysis data: near-surface (2 m) air temperature (SAT), zonal winds, sea-level pressure, and turbulent fluxes from the ERA5 reanalysis (Hersbach et al., 2020); precipitation rate from the version-2 GPCP dataset (Adler et al., 2003); cloud cover from the version-3 ESA Cloud_cci dataset (ESA CCI-CLOUD; Stengel et al., 2020); potential temperature and salinity of the ocean from the Hadley Center EN4 (version 4.2.2; Good et al., 2013); sea ice concentration from OSI SAF (OSI-409/OSI-409-a; EUMETSAT Ocean and Sea Ice Satellite Application Facility, 2015); and sea ice volume from GIOMAS (Global Ice-Ocean Modeling and Assimilation System; Zhang and Rothrock, 2003). The period of comparison maximizes data availability and is therefore 1980–2014 for all the

 12

cases, except ~~but~~ for the GPCP dataset (1983–2014) and the ESA CCI-CLOUD dataset (1982–2014). Biases in sea-surface temperature (SST) are very similar to those in SAT and are therefore not shown.

3. Results

3.1 Spin-up phase

Across all three model resolutions, the length of the spin-up (50 years) appears to be insufficient to equilibrate the full ocean (Fig. 3b); in fact; the ocean temperature is still drifting about 0.001–0.002 °C/yr (computed over the last 50 years) towards warmer conditions at the end of the control simulation in the three configurations. In the upper ocean, however, VHR shows the smallest warming drift of the three configurations: about 0.00005 °C/yr compared to 0.0025 °C/yr and 0.0062 °C/yr in HR and LR, respectively (computed over the last 50 years; Fig. 3a). It is therefore safe to say that an analysis focused on the upper ocean and on the air–sea interface will feature~~enjoy~~ a relatively stable climate in the control simulations. In the historical simulations, the warming of the ocean accelerates due to the CO_2 forcing; after 64 years (year 114 in Fig. 3), the whole ocean warming reaches similar values to those at the end of the control simulations after 100 years in the three model resolutions. Near the surface, the warming trend is much larger. Of the three configurations, VHR is the one with the smallest drift in the control run and the smallest ocean warming in the historical period. Although the three runs start from similar initial conditions derived from an EN4 climatology (Section 2.3), VHR is ~0.4 °C warmer near the surface than LR and HR, especially over the spin-up period. This is likely related to the development of a widespread warm bias over the Southern Ocean (Fig. 4), which we discuss in detail in Section 3.6. The trends in global salinity at the end of the control simulations are all smaller than 0.00005 psu/yr (computed over the last 50 years; not shown); the three configurations are thus still drifting slightly. As found for the temperature, VHR also shows the smallest drifts out of the three configurations (not shown).

In the following Sections, we describe the main characteristics of the VHR compared to LR and HR by focusing on particular regions and biases. This approach should help us highlight the benefits, or lack thereof, due to increased resolution. The main biases in the three model configurations are compared with the observational data set listed in Section 2.4.

 13

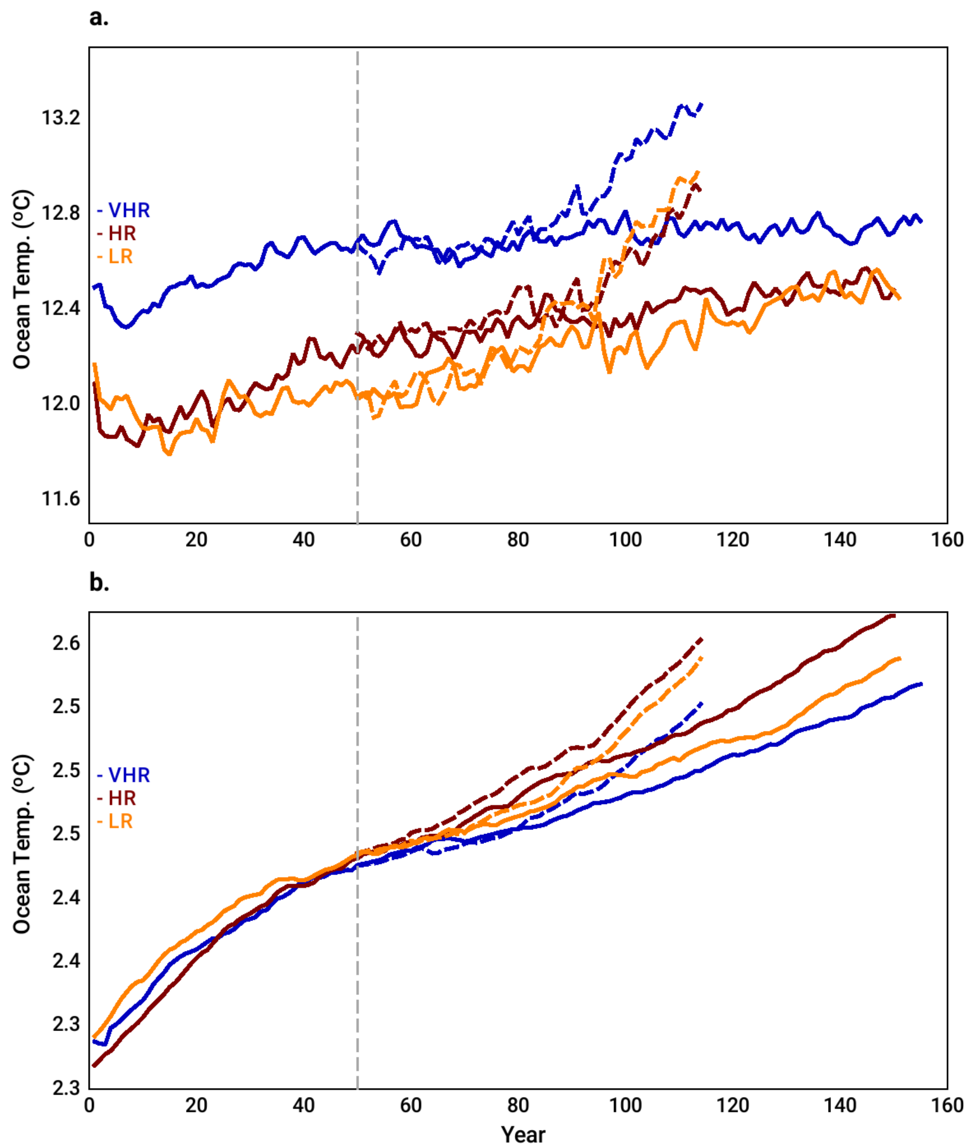

Figure 3. Mean oceanic temperature (in °C) in the LR (yellow), HR (red), and VHR (blue) models in the spin-up runs (0–50-year period), control runs (50–150-year period; solid lines), and historical runs (50–114-year period; dashed lines) in a) the upper 100 m, and b) the whole ocean. The vertical dashed line marks the end of the spin-up period.

3.2 Tropics

A warm bias of 1–2 K is present over the subtropical upwelling regions along the South American and African coasts in the three configurations and shows small variations across them (Fig. 4). The increase in resolution in VHR has thus no clear benefit to reduce it. Past studies

14

have related this bias to an underestimation of the stratocumulus cloud deck (Richter, 2015). This also seems to be the case in the three models, which all show negative cloud biases by about 20 % over all the subtropical upwelling areas, specially along the subtropical Pacific and Atlantic western coasts (Fig. 5). A better resolved orography near the region does not contribute to reducing the bias either, as suggested in previous studies (Milinski et al., 2016): for example, although VHR shows reduced temperature biases along the Andes compared to HR and LR, it has no effect on the biases over the eastern subtropical Pacific upwelling.

Overall, VHR shows reduced tropical precipitation biases compared to HR and LR (Fig. 6). This is the case, for example, for the double ITCZ bias: this bias is usually characterized by a precipitation excess over the central tropical North Pacific and the western tropical South Pacific and a precipitation deficit over the equatorial Pacific, as LR clearly shows. The dry area over the Equator is reduced with resolution, and the anomaly is even non-significant in VHR. This is a clear improvement from increased resolution, and it can be related to a reduced cold bias over the Equator (Fig. 4). In contrast, the precipitation excess over the tropical North Pacific and the Maritime Continent persists into VHR, with only minor reductions of 1–2 mmd^{-1} compared to HR and LR (Fig. 6). The precipitation excess over the tropical North Pacific suggests a seasonal cycle reaching too far north, while the excess over the Maritime Continent, together with that over the western tropical Atlantic and Indian oceans, suggests an excess in convective precipitation over very warm waters.

Over the tropical Atlantic, the precipitation bias pattern points to an ITCZ anchored to the south-western part and not reaching the Sahel area. This bias is somewhat reduced in VHR compared to HR and LR, although not entirely removed. Over land, the dry bias over North Brazil, which has been linked to a misrepresentation of the seasonal cycle and extreme events in CMIP6 models (Monteverde et al., 2022), as well as ~~and~~ the wet bias along the Andes are not reduced with resolution, either. These positive and negative precipitation biases appear together with positive and negative biases in cloud cover, respectively, related to an overestimation or underestimation in convective clouds (Fig. 5).

15

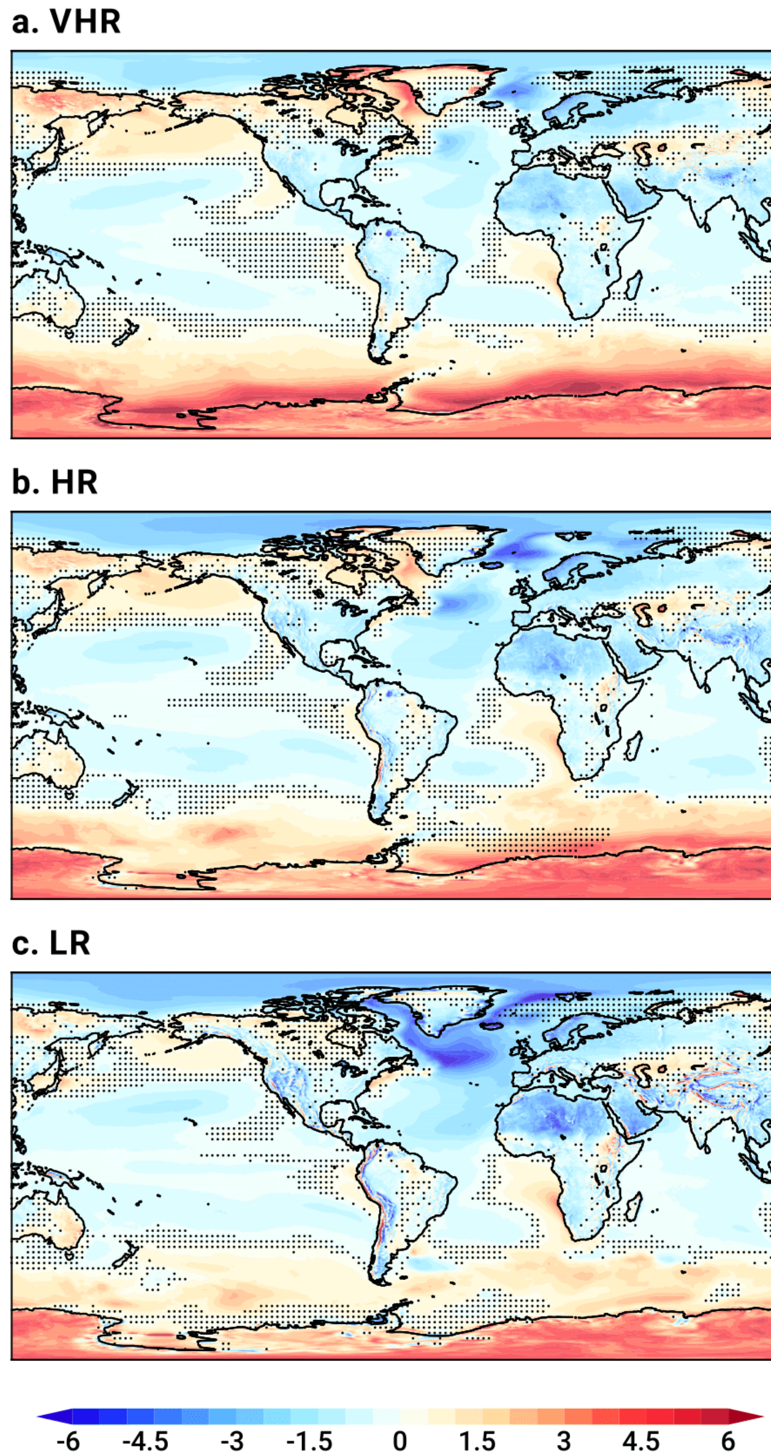

Figure 4. Bias in SAT (in K) with respect to ERA5in the a) VHR, b) HR, and c) LR models for the period 1980–2014. Stippling masks anomalies that are not significant at the 5 % level.

 16

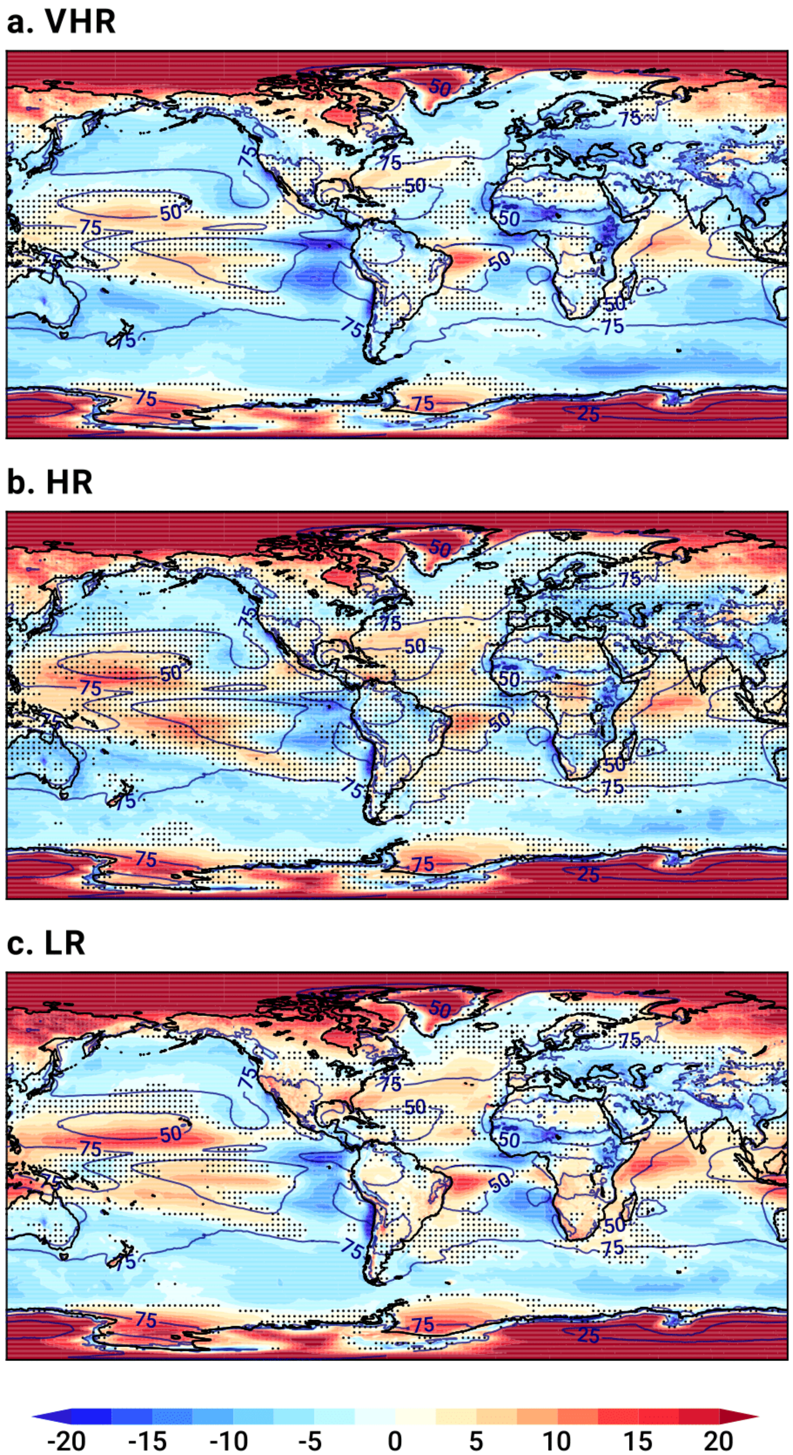

Figure 5. Bias in cloud cover (in %) with respect to ESA CCI-CLOUD (contours in all the panels; in %) in the a) VHR, b) HR, and c) LR models for the period 1982–2014. Stippling masks anomalies that are not significant at the 5 % level.

17

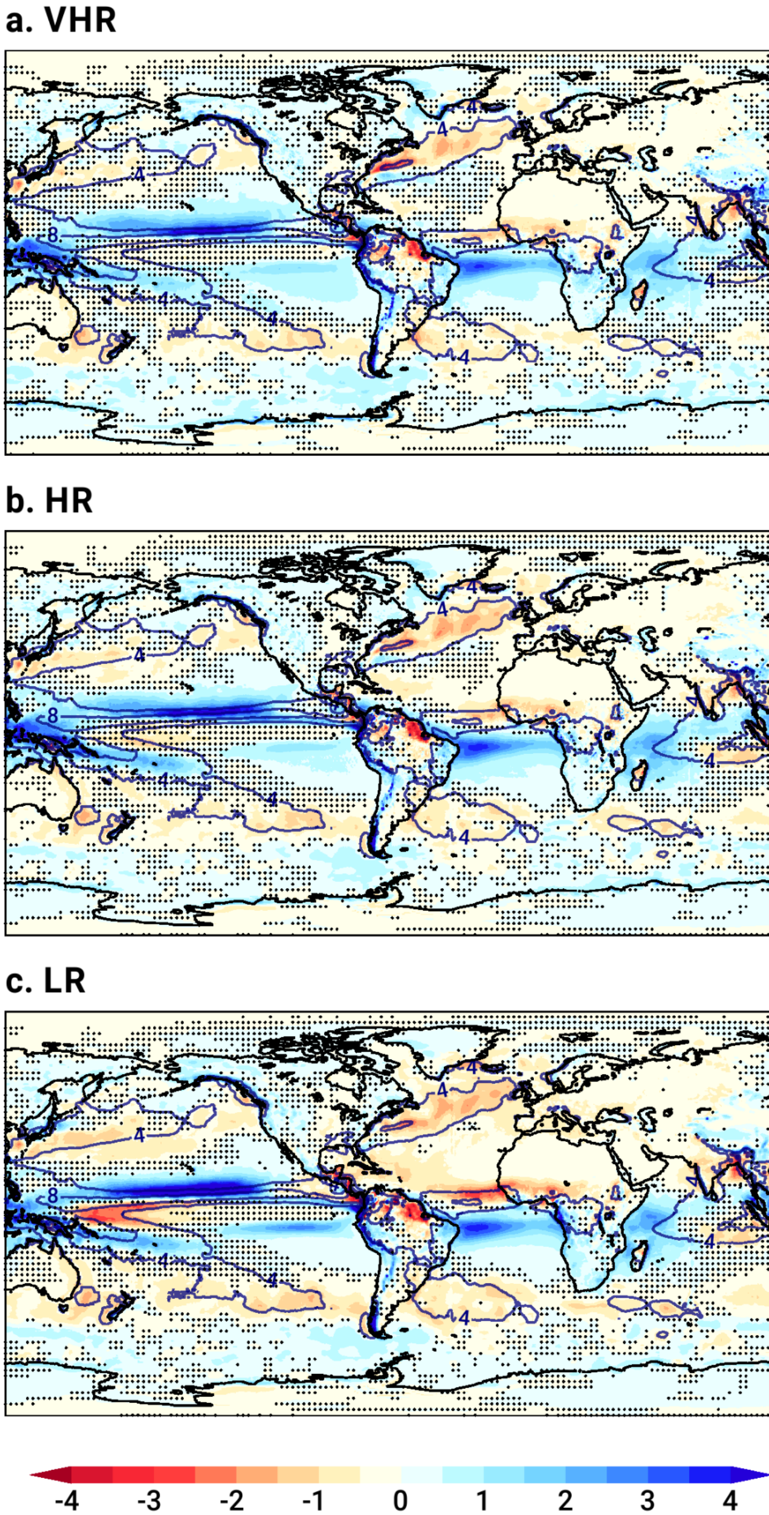

Figure 6. Bias in precipitation rate (in mmd^{-1}) with respect to GPCP (contours in all the panels; in mmd^{-1}) in the a) VHR, b) HR, and c) LR models for the period 1983–2014. Stippling masks anomalies that are not significant at the 5 % level.

18

3.3 Northern Hemisphere mid- and high-latitudes

The largest improvement in the simulated climate from LR to VHR is over the North Atlantic. From south to north, the Gulf Stream representation is much improved in VHR compared to HR and LR, with sharper gradients in temperature and sea-surface height (not shown). The position of the Gulf Stream separation is also improved, which leads to a reduction of the warm bias along the US East Coast from LR to VHR (Fig. 4). A paper on a dedicated analysis of the biases over the North Atlantic along the Gulf Stream is currently in preparation.

Farther north, the widespread cold bias up to about 6 K in LR is strongly reduced in HR, and even further in VHR, which is the configuration closest to observations (Fig. 4). The cold bias in LR is related to an unrealistically large sea ice extent, which covers the entire Labrador Sea and the western part of the subpolar North Atlantic (Figs. 7 and 8). The reduction of the cold bias between LR and VHR ~~bias~~ has a deep impact on the climate of the North Atlantic. In the atmosphere aloft, it improves the representation of the boreal winter (DJF) stormtrack (Fig. 9) and jet (Fig. 10). The boreal winter stormtrack is overestimated over the subpolar North Atlantic, particularly over the eastern part, in LR, likely related to an excessively strong meridional temperature gradient; by contrast, VHR stormtrack is much closer to ERA5 over the North Atlantic. In the ocean, excessive sea ice leads to a negative salinity bias above 2 psu in the subpolar North Atlantic in LR, which is much reduced in VHR (Fig. 11). Two mechanisms can explain this fresh bias in LR: on the one hand, a reduced oceanic salinity transport from subtropical latitudes by a weakened subpolar gyre (not shown); on the other, errors in the seasonal cycle of the sea ice, during which ice melting would cause an anomalous freshwater input in regions where it is not observed. The negative bias in surface salinity propagates into deeper levels, especially between 300 m and 1000 m in the Arctic (Fig. 12). Similarly, the warm subsurface bias at around 40–50 °N might also be related to the sea ice excess in the subpolar North Atlantic in LR (Fig. 11). Expanded sea ice in LR causes weaker subpolar gyre strength and associated northward heat transport (not shown), leading to heat accumulation in the intergyre region. However, although this bias is reduced at higher resolutions in HR and VHR, it is still present, suggesting other deficiencies in the formation of intermediate waters in the North Atlantic. The overly large sea ice cover also hampers oceanic deep mixing in the Labrador Sea in LR, whose main region of deep water formations are in the Nordic Seas instead (Fig. 13). Oceanic deep mixing takes larger values above 1000 m in VHR and HR in the Labrador Sea. A detailed analysis of the characteristics and driving mechanisms of the deep water formation in the Labrador Sea across the three resolutions and compared to observations is currently in preparation.

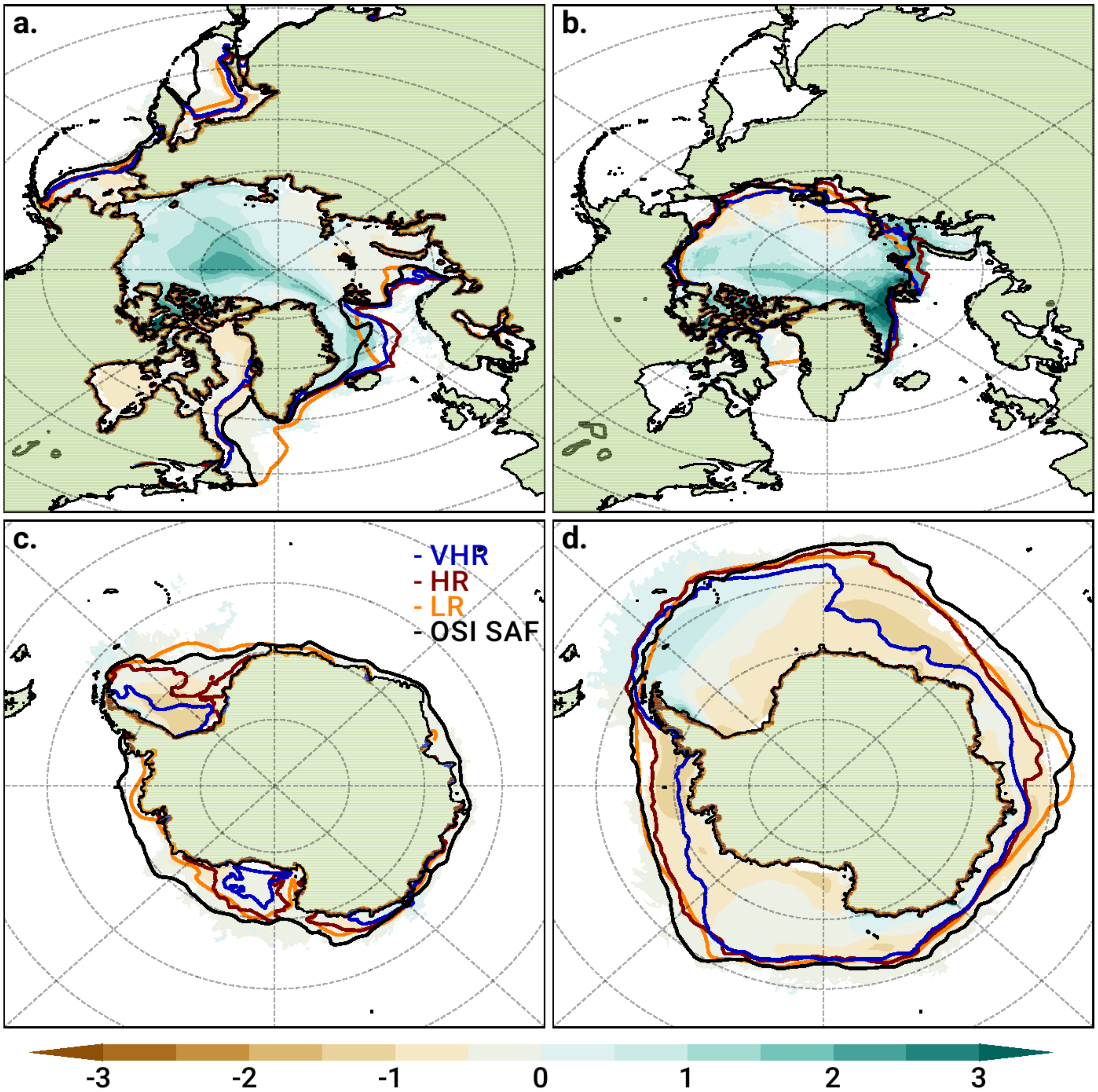

Figure 7. Bias in sea ice thickness (in m; shading) in VHR with respect to GIOMAS for the period 1980–2014. Colored c~~Sea ice concentration (in % of area) in the VHR model (gray shading) for the period 1980–2014. C~~ontours are the 15-% value of the sea ice concentration in the LR (orange), HR (red), and VHR (blue) models, as well as in OSI SAF (black) for the period 1980–2014. a,b~~Top/bottom panels~~ are for the Arctic, while c,d are for ~~/~~Antarctica in March (a,c~~left~~) and September (b,d~~right~~).

20

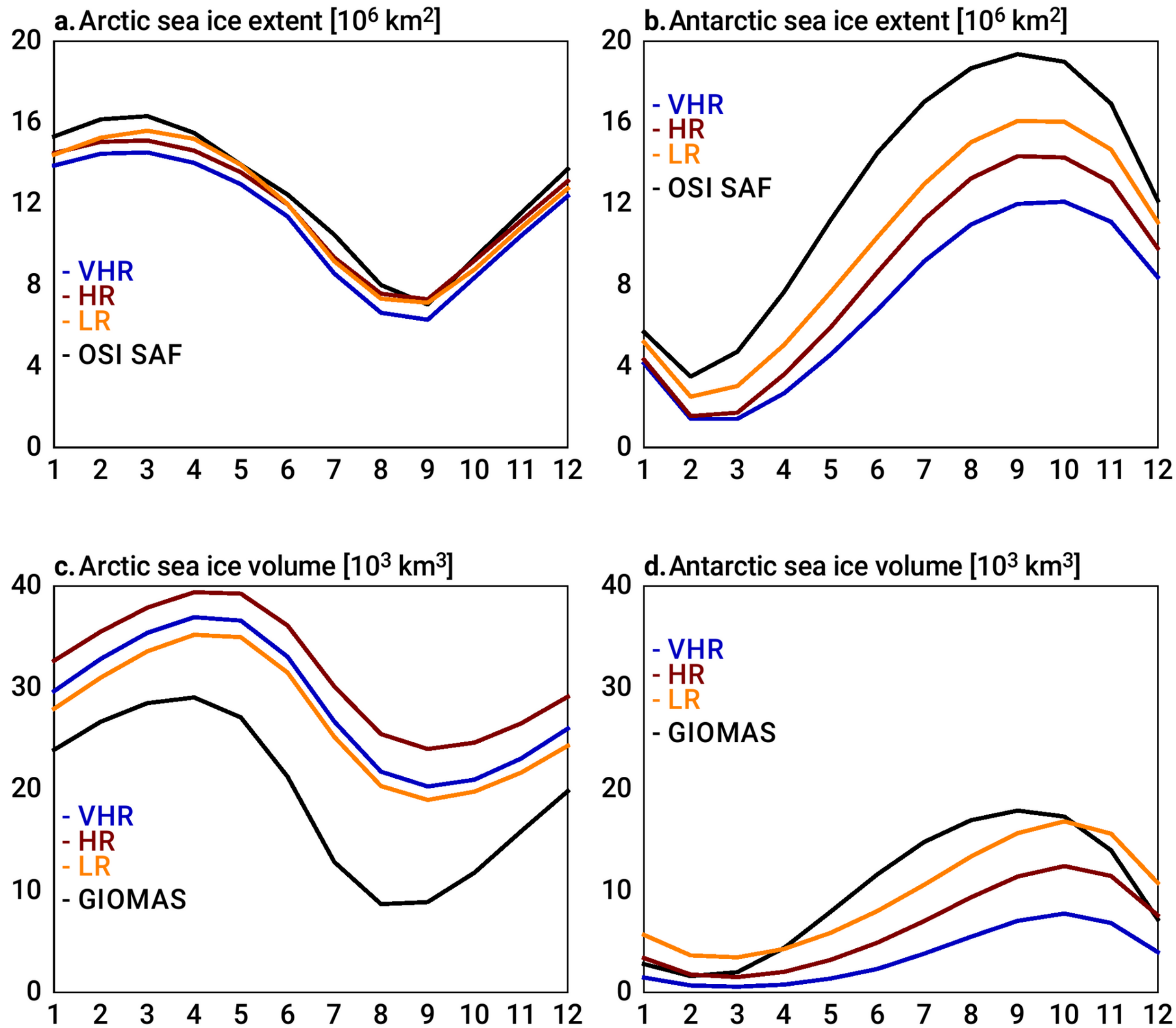

Figure 8. Monthly climatology in the sea ice extent (in 10^6 km^2; a,b~~top~~) and volume (in 10^3 km^3; c,d~~bottom~~) in the Arctic (left) and Antarctica (right) in the LR (yellow), HR (red), and VHR (blue) models, as well as in OSI SAF, for sea ice extent, and GIOMAS, for the volume, for the period 1980–2014.

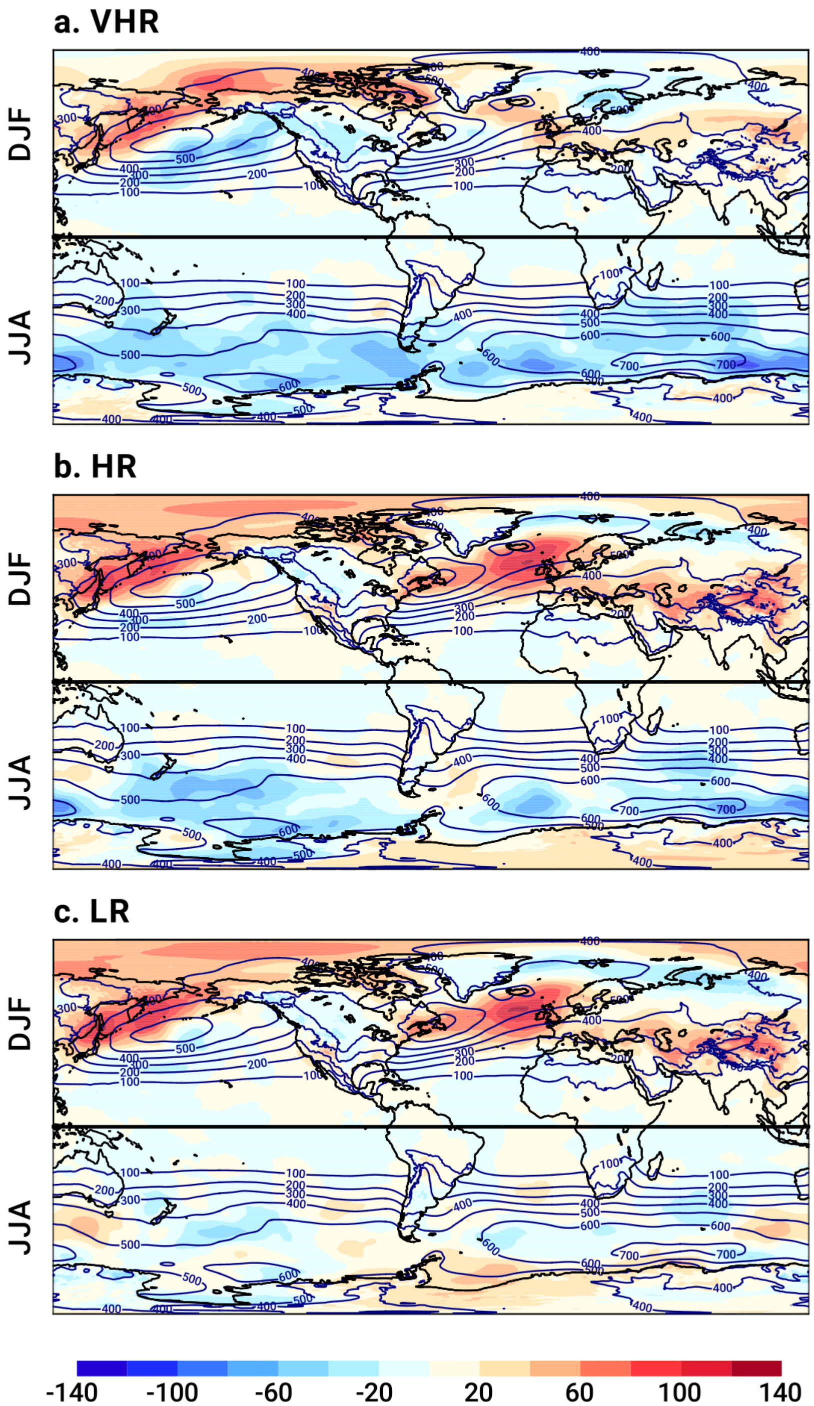

Figure 9. Bias in winter stormtrack, computed as the standard deviation of the 2–6 d band-pass filtered daily sea-level pressure (in Pa) with respect to ERA5 (contours in all the panels; in Pa) in the a) VHR, b) HR, and c) LR models for the period 1980–2014. Each panel show anomalies in the boreal winter (DJF; top) and austral winter (JJA; bottom).

22

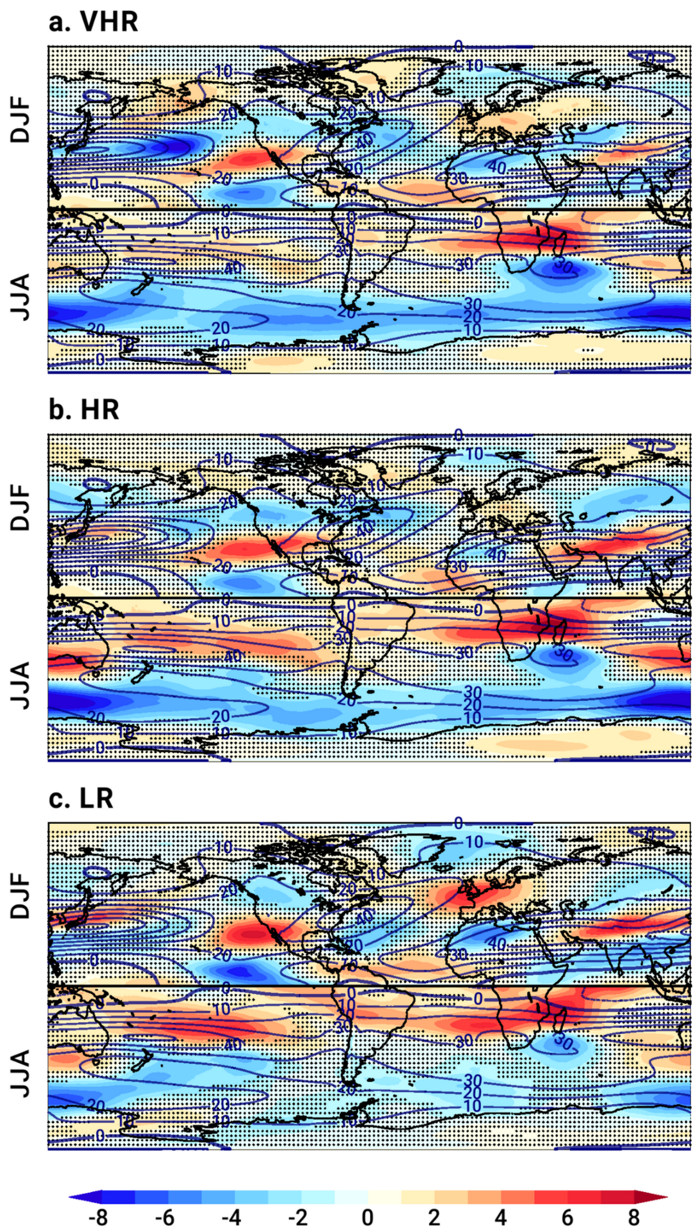

Figure 10. Bias in winter zonal wind at 250 hPa (in ms^{-1}) with respect to ERA5 (contours in all the panels; in ms^{-1}) in the a) VHR, b) HR, and c) LR models for the period 1980–2014. Stippling masks anomalies that are not significant at the 5 % level. Each panel show anomalies in the boreal winter (DJF; top) and austral winter (JJA; bottom).

23

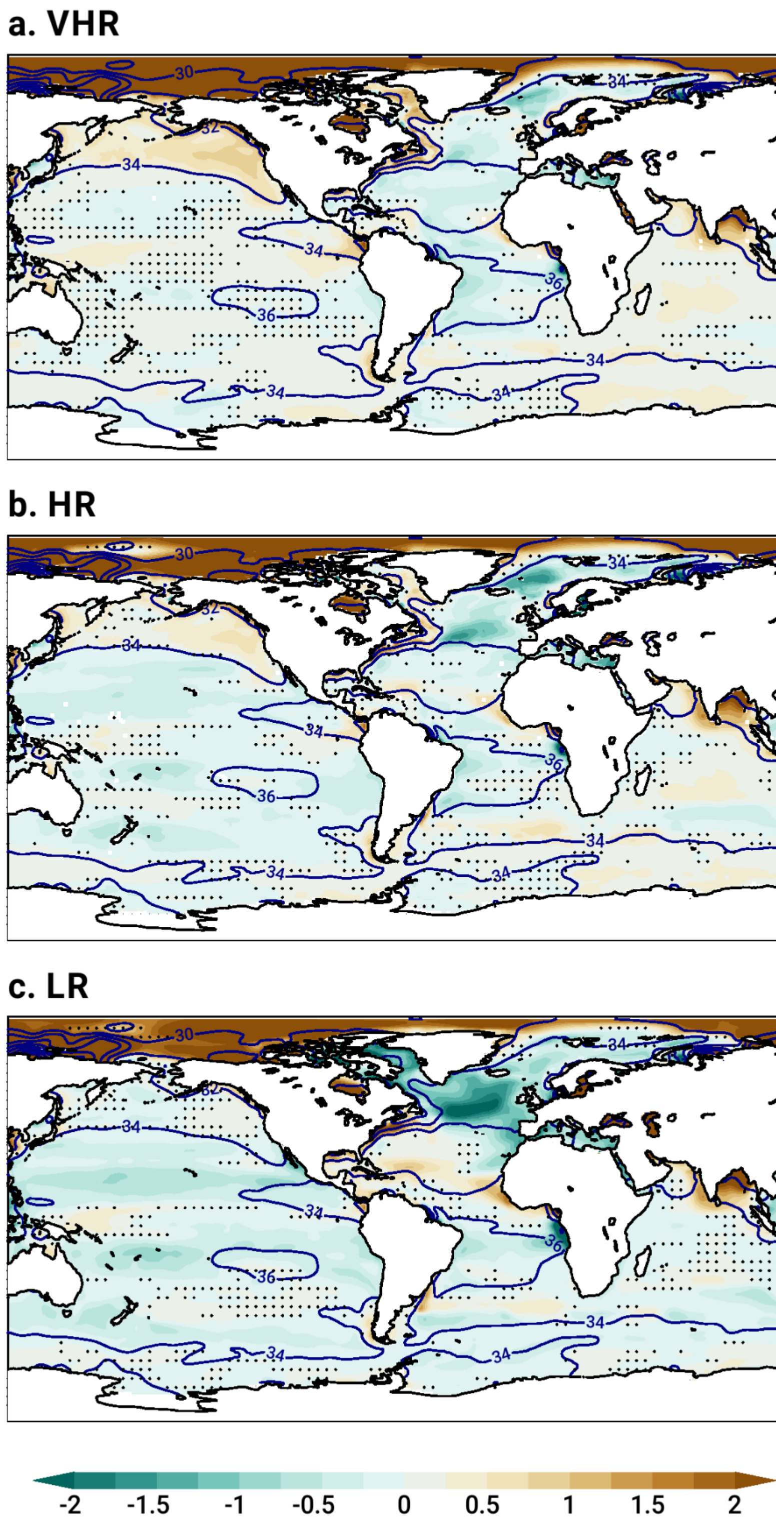

Figure 11. Sea-surface salinity bias (in psu) with respect to EN4 (contours in all the panels; in psu) in the a) VHR, b) HR, and c) LR models for the period 1980–2014. Stippling masks anomalies that are not significant at the 5 % level.

24

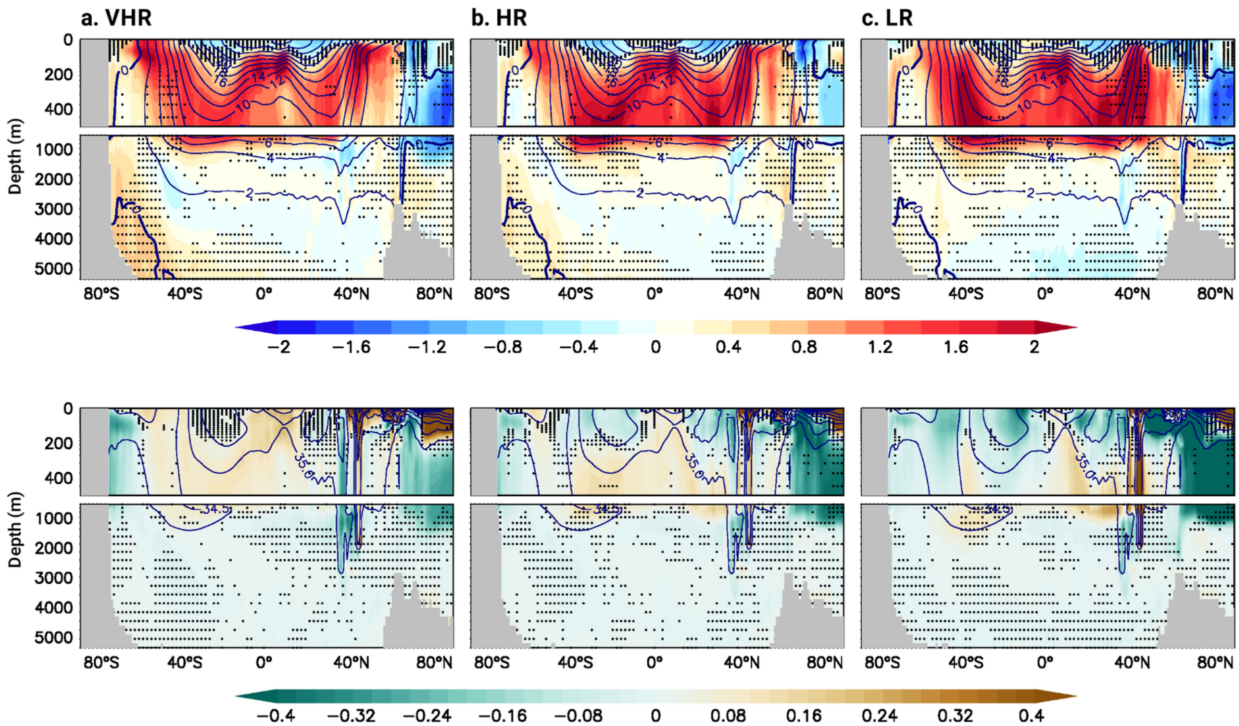

Figure 12. Bias in ocean potential temperature (in K; top) and in salinity (in psu; bottom) with respect to EN4 (contours in all the panels; in K, top, and psu, bottom) in the a) VHR, b) HR, and c) LR models for the period 1980–2014. Stippling masks anomalies that are not significant at the 5 % level. Each panel is separated into the upper and lower 500 m.

 25

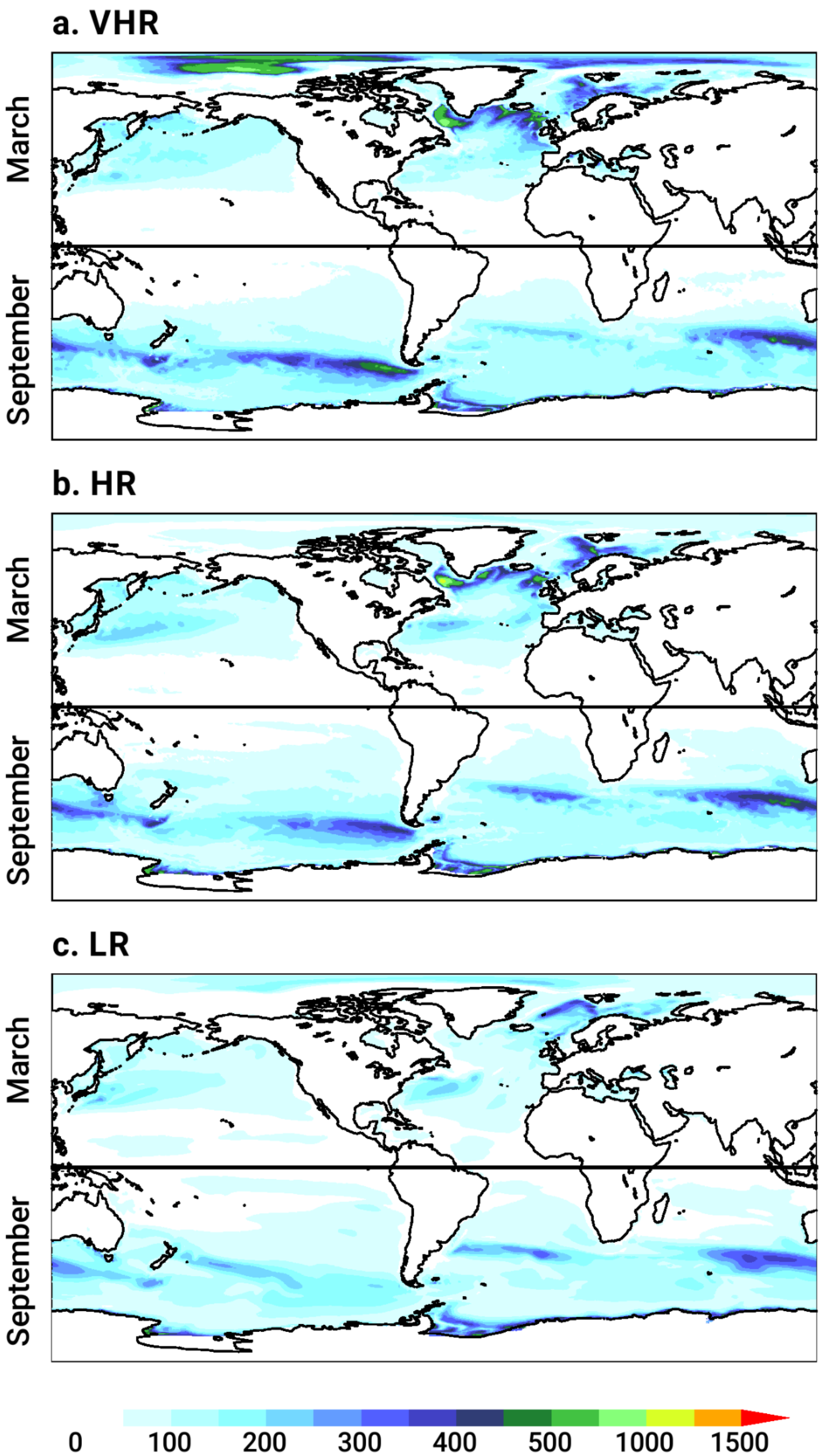

Figure 13. Mixed layer depth (in m) in the a) VHR, b) HR, and c) LR models for the period 1980–2014. Northern Hemisphere and Southern Hemisphere values are for March and September, respectively.

26

Weak deep mixing results in a relatively weak Atlantic Meridional Overturning Circulation (AMOC; Fig. 14) in LR. The AMOC strength increases with resolution, related to the reduction of the cold bias and sea ice extent bias over the subpolar North Atlantic. The strength of the AMOC in VHR is thus the closest to the observed RAPID strength at 26 °N (17 ± 3 Sv, corresponding to the mean and standard deviation, respectively; Frajka-Williams et al., 2019) among the three models: 14 ± 3 Sv in VHR, 12 ± 4 Sv in HR, 11 ± 2 Sv in LR (computed from monthly streamfunction at 26 °N for the period 2004–2014). The structure of the AMOC cell is similar in the three model configurations, with a main positive cell in the upper 3000 m up to 60 °N and with a maximum at around 30 °N, and a negative deeper one below with a strength of 2–4 Sv.

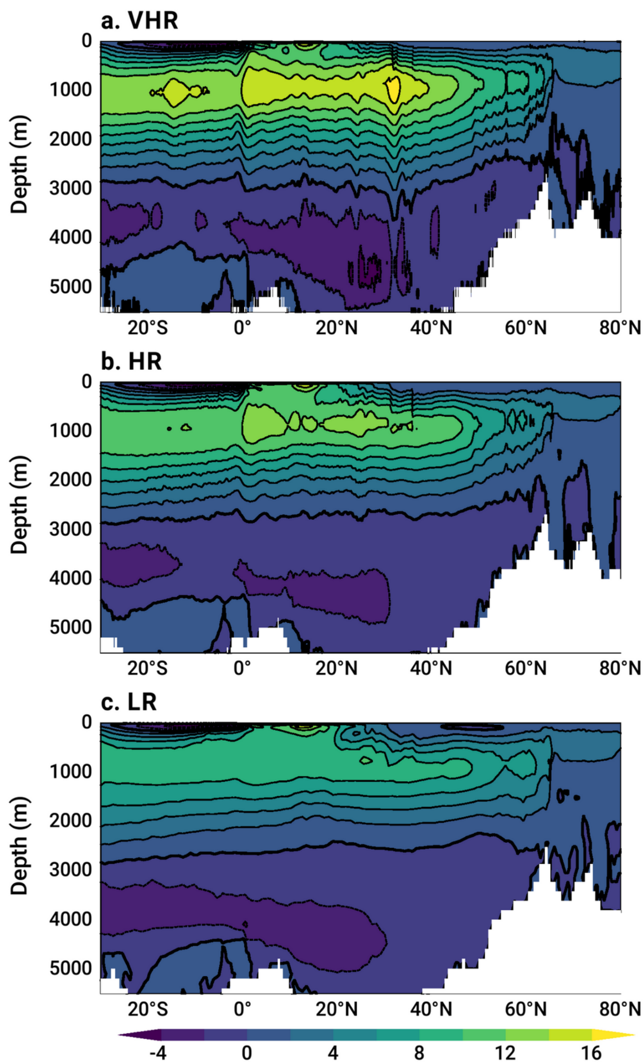

Figure 14. Atlantic overturning streamfunction (in Sv) in the a) VHR, b) HR, and c) LR models for the period 1980–2014.

27

In HR, and even more in VHR, the cold bias over the Labrador Sea is replaced by a warm bias (Fig. 4), up to 3–4 K in VHR. This bias also appears in other eddy-rich climate models, related to a stronger ocean heat transport than at lower resolutions in the Atlantic (Roberts et al., 2020b). Over the Nordic Seas, by contrast, a cold bias is present in the three models, although it is somewhat reduced at VHR by 1–2 K compared to LR and HR (Fig. 4). In the three cases, this bias is related to an excessively large sea ice cover in the region (Fig. 7). The warm bias over the Labrador Sea and cold bias over the Nordic Seas in VHR might suggest a misrepresentation of the distribution of oceanic heat transport between the two basins, favoring the westward transport over the northward across-Ridge heat transport. It might also or instead be related to a misrepresentation of the sea ice drift across the Denmark Strait (Gutjahr et al., 2022). Relatively weak transport across the Strait would lead to ice deficit in the Labrador Sea, and hence warming, and to ice accumulation in the Nordic Seas, hence cooling.

On a hemispheric scale, the three models simulate a slightly low Northern Hemisphere sea ice extent, mainly due to the underestimation of the sea ice cover in the Sea of Okhotsk, Baltic Sea, and Labrador Sea in HR and VHR (Fig. 8). By contrast, the three models show an overly large sea ice volume by about 10^4 km^3 compared to GIOMAS (Fig. 9), as they all simulate very thick sea ice in the central Arctic (Fig. 7 for VHR~~not shown~~). Anomalously thick ice in the central Arctic would~~models~~ lead~~s~~ to an excess of brine rejection (not shown), which can explain the positive salinity bias above 2 psu in the upper 100–200 m of the Arctic Ocean (Figs. 11 and 12). In VHR, the associated increase in upper-ocean density leads to deeper oceanic mixing than in LR or HR, with a mixed layer depth in the central Arctic that can reach up to 1000 m (Fig. 13).

Over the Pacific, biases tend to be weaker than over the Atlantic. A warm bias of about 1 K develops over the subpolar North Pacific from LR to VHR (Fig. 4), which could explain the negative bias in boreal winter (DJF) stormtrack aloft (Fig. 9) and the weaker jet stream over the central Pacific in VHR (Fig. 10).

Over land, the cold bias over the Sahara is reduced with increased resolution (Fig. 4). Similarly, the cold biases over large mountain ranges, such as the Rockies, the Andes, and the Himalaya, up to about several degrees in LR are much reduced in VHR (Fig. 4), related to better resolved orography.

28

3.4. Southern Ocean

The Southern Ocean is the region where VHR performs the worst compared to HR and LR. The warm bias over the Southern Ocean increases with resolution, up to 4–5 K in VHR, compared to 1–2 K and 2–3 K for HR and LR respectively (Fig. 4). It tends to be largest over the Atlantic and Indian sectors of the Southern Ocean and close to the Antarctic coast. Although the warm bias remains generally confined to the upper 100–200 m at around 60 °S, it might also be connected to the warm bias at depth between 2000 m and 4000 m (Fig. 12).

Two main mechanisms could explain the Southern Ocean warm bias: VHR has the largest cloud cover underestimation of the three models, especially over the Atlantic and Indian sectors, up to 15 % in VHR compared to 5–10 % in LR and HR (Fig. 5). Previous studies have related the Southern Ocean warm biases to misrepresentation and underestimation of the mixed-phase clouds, which lead to an excess of shortwave radiation reaching the surface, thereby warming it (e.g., Hwang, and Frierson, 2013; Hyder et al., 2018). Connected to the warm bias, VHR also shows the lowest sea ice extent of the three resolutions all year round (Figs. 7 and 8). Although the three models underestimate the Antarctic sea ice extent, in VHR this is nearly half as in observations for the same period (OSI SAF, 1980–2014). In terms of sea ice volume (Fig. 8), however, LR shows larger values by about $2 \cdot 10^3$ km^3 than GIOMAS between November and April, pointing to overly thick sea ice. As for the extent, VHR also shows the lowest sea ice volume, nearly half of the values in GIOMAS. The three models show the maximum volume one month later than in GIOMAS, in October rather than in September. This contrasts with the Arctic, where the three models capture the general shape of the seasonal cycle.

The surface warming over the Southern Ocean leads to a widespread underestimation of the stormtracks (Fig. 9) and jet stream (Fig. 10) in the austral winter (JJA) in HR and, especially, in VHR, compared to LR, which is much closer to ERA5. Although precipitation is also underestimated over the Southern Ocean, specially in VHR, this is not a particularly strong bias, at least compared to those over the tropical regions (Fig. 6).

Late austral summer (September) deep mixing tends to increase by about 200 m from LR to HR and VHR, especially in the Pacific sector. These two latter resolutions show similar deep mixing mean state, with variations only due to resolution and the better representation of the

29

mesoscale in VHR (Fig. 13). The underestimation of the stormtrack over the Southern Ocean therefore does not seem to have an impact on the oceanic mixing below in VHR.

3.5 Air–sea coupling

We compare the change in the intensity of air–sea coupling from LR to VHR via the computation of cross-correlation coefficients of the deseasonalized monthly SST and net surface energy flux (Fig. 15). This analysis has extensively been used to study regions in which the ocean tends to drive atmospheric variability (correlation coefficient values approaching one) or vice versa (correlation coefficient values close to zero; e.g., Bishop et al., 2017; Small et al., 2019). The three model configurations are compared with the ERA5 reanalysis, as done in the previous s~~S~~ections for the biases. To complement the analysis with a non-model based product, we also include satellite observations of radiative fluxes from J-OFURO3 (Tomita et al., 2019). The two products show an overall good agreement, with areas of large correlation coefficient values at the Equator, along the western boundary currents, and over the Southern Ocean (Fig. 15a,b). These areas, nonetheless, tend to be broader in J-OFURO3 than in ERA5.

Over the tropics, the three configurations tend to underestimate the coupling around the Equator, although they all reproduce well the band of correlation coefficients of high values along the equatorial Pacific and Atlantic. However, this band is narrower in LR and HR over the subtropics than it is in ERA5 and J-OFURO3. VHR is thus the closest configuration to the two reference observational products in the region. This result highlights the need for a model resolution finer than 25 km in both the ocean and atmosphere to represent realistic tropical climate interactions, in agreement with conclusions in Section 3.2.

At mid-latitudes, the coupling is greatly improved in HR and VHR compared to LR, particularly over the subpolar regions compared to ERA5 and J-OFURO3. LR shows a rather smooth pattern, with very low values in key regions over the Gulf Stream, Kuroshio Current, and Southern Ocean, which suggests a standard 1° resolution is insufficient to represent a realistic air–sea coupling. VHR and HR show, by contrast, sharper gradients in the correlation coefficient values close to 1 over those regions. This result is consistent with previous studies, which also found a degradation of the air–sea coupling in coarse grids, especially above 1° (e.g., Small et al., 2019). However, VHR shows unrealistic broader areas of higher correlation coefficient values than ERA5 and J-OFURO3 at mid-latitudes, degrading results from HR. One hypothesis for this discrepancy might result from the difference of IFS grid resolution between VHR

(T1279) and ERA5 (T639), since the relationship between SST and turbulent fluxes shows certain scale dependency (e.g., Small et al., 2019; Sun and Wu, 2022). However, results do not improve even when regridding VHR onto ERA5 grid before computing the correlation coefficients (not shown). A second hypothesis is the lack of the ocean current feedback in VHR, hence the lack of eddy-killing, which can control the simulated Gulf Stream's dynamics and energy pathways (Renault et al., 2023). However, the pattern of correlation coefficient values remains relatively unchanged when it is computed with a VHR configuration that includes a parameterization that considers the wind adjustment to the ocean current feedback (not shown) (Renault et al., 2019). The results suggest that the VHR's ocean exerts a stronger and more widespread influence on the atmosphere variability than in HR and LR.

Further north, air–sea coupling is overestimated in all the models over the Nordic Seas, likely related to the excess in sea ice in the region and its changes over the seasonal cycle. Together, the results suggest that a realistic air–sea coupling requires grids finer than 1/4° at least, with potential local improvements on a 1/12° grid, especially over the Tropics.

4. Discussion and Conclusions

This paper presents the eddy-rich configuration of the EC-Earth3P-VHR global model for HighResMIP. We describe both the necessary technical developments to run the model efficiently, and the main features of the simulated climate compared to recent observations (1980–2014 period) and to two lower-resolution model configurations (the eddy-present, ~25-km-grid EC-Earth3P-HR; and the non-eddy, ~100-km-grid EC-Earth3P-LR). The EC-Earth3P-VHR (or VHR) uses a comparable atmospheric and oceanic resolution of 10–15 km in a global fully coupled setup, which is, to our knowledge, one of the finest combined grids ever used to date to perform long climate integrations for CMIP (e.g., Small et al., 2014, Chang et al., 2020). Our focus here is on the HighResMIP historical simulation (HighResMIP's hist-1950). This run is part of a larger set of runs, which includes a spin-up and control runs (HighResMIP's control-1950), a future extension under the ssp8.5 scenario (HighResMIP's highres-future), three hosing simulations forced by idealized Greenland melting, and AMIP sensitivity simulations, all performed within the European PRIMAVERA project and the Spanish STREAM project. Those additional simulations will be described in their corresponding publications, which are currently in preparation.

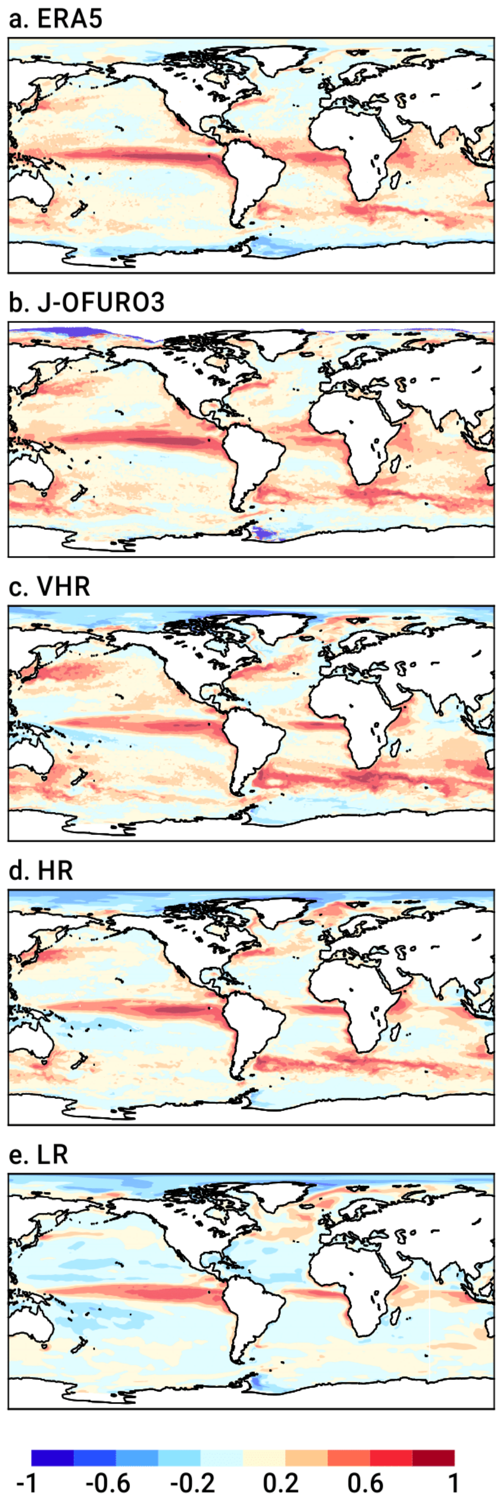

Figure 15. Cross-correlation coefficients between monthly SST and net surface energy flux for the period 1980–2014 in a) ERA5, b) J-OFURO3, and in the c) VHR, d) HR, and e) LR models. The seasonal cycle and linear trends are removed from the monthly SSTs and energy fluxes before the correlation coefficients are computed. This is done on the original grid in all the cases.

 32

The comparison across the three resolutions (this is, VHR, HR, and LR), all with the same physics and no additional tuning, allows identifying regions where increased resolution improves the model performance with respect to observations. One of those regions is the Tropics, and specially the equatorial Pacific, where the cold tongue bias and the dry bias above are both reduced in VHR compared to HR and LR. Wengel et al. (2021) also reports a similar bias reduction in an eddy-resolving configuration of the CESM (0.25° resolution in the atmosphere, 0.1° resolution in the ocean), which they link to better represented mesoscale features, such as tropical instability waves. Similarly, the HadGEM3-GC3.1 global model shows a reduced dry bias over the equatorial Pacific in its configuration with a 1/12° ocean and a 50-km atmosphere (Roberts et al., 2019). By contrast, the eddy-rich MPI-ESM1.2-ER global model (1/12° ocean as well) shows no evident changes in equatorial precipitation when coupled to a 100-km atmosphere (Gutjahr et al., 2019). Combined, these results suggest that resolutions finer than 25–50 km might be needed in both the atmosphere and ocean to improve surface coupling and reduce biases. However, minimizing equatorial precipitation biases might actually be much more complex than simply increasing model resolution, as found for the ICON global atmosphere–ocean model with a uniform grid spacing of 5 km. Despite its high atmosphere and ocean resolutions, this model still exhibits a strong dry bias over the equatorial Pacific driven by a surface cold bias underneath (Hohenegger et al., 20232; Segura et al., 2022). This model, however, is not directly comparable to those other HighResMIP models, as it includes a minimum set of parametrization. Thus, while convection is directly resolved in ICON, it is parametrized in VHR and the listed models. The incorrect representation of the equatorial SST structure in ICON might instead be related to unresolved sub-grid processes (Segura et al., 2022).

The Gulf Stream is another region in which increased model resolution is beneficial, with a reduced temperature biases over the separation region and the central North Atlantic in VHR compared to HR and LR. Such improvements have been related to the resolving of the first baroclinic Rossby radius of deformation over most of the region and/or the exceeding of a critical Reynolds number (e.g., Chassignet and Marshall, 2008) and have been linked to the increase in resolution over the shelf areas to the north of the Gulf Stream (Sein et al., 2017). Similar results have also been reported for the HadGEM3-GC3.1 (Roberts et al., 2019) and MPI-ESM1.2-ER (Gutjahr et al., 2019) global models, both with a 1/12° oceanic grid but coarser

 33

atmospheric grids (~50 km and ~100 km, respectively). This suggests that oceanic resolution is a critical factor for the Gulf Stream representation. Nonetheless, other model features might also be relevant to simulate a realistic Gulf Stream, as no improvement is found in the CESM1.3 model between a 1°- and a 0.1°- oceanic grid, for which the Gulf Stream separation occurs too far north (Chang et al., 2020). One of the many potential reasons behind the discrepancy might be the obvious difference in the number of atmospheric vertical levels: 91 in VHR, 85 in HadGEM3-GC3.1 (Roberts et al., 2019), 95 in MPI-ESM1.2-ER (Gutjahr et al., 2019), but only 30 in CESM1.3 (Meehl et al., 2019), which is expected to degrade the representation of key stratosphere–troposphere interactions affecting North Atlantic variability, and, by extension, the wind field, which is critical for the Gulf Stream separation. As nicely summarized in Chassignet and Marshall (2008), however: "The Gulf Stream separation, indeed, turns out to be quite sensitive to a variety of other factors such as subgrid scale parametrization, subpolar gyre strength and water mass properties, [deep western boundary current] strength, representation of topography, and the choice of model grid". A realistic representation of the Gulf Stream is crucial for the North Atlantic and European climate. SST biases in the Gulf Stream can drive not only local changes over the North Atlantic, but a large-scale dynamic response over remote regions of the Northern Hemisphere through a quasi-zonal planetary barotropic Rossby wave response (Lee et al., 2018). Similarly, a more realistic, farther-south Gulf Stream has been shown to shift north in simulations with increased CO_2 in models at eddy-rich resolutions (Saba et al., 2016; Moreno-Chamarro et al., 2021). This shift would lead to amplified warming of the US East coastal region, which might be consistent with the anomalous warming observed in the Gulf Stream area in recent decades (Pershing et al., 2015; Todd and Ren, 2023). Reducing biases in the Gulf Stream area is therefore key to reproducing a realistic atmospheric circulation and to the sensitivity of the response to an external forcing.

Mainly related to increased atmospheric resolution, VHR also shows reduced precipitation biases over mountain ranges all over the world. This suggests VHR might provide more realistic regional information of precipitation variability and future changes than lower resolution models can. Giorgi et al. (2016), in fact, showed that increased model resolution leads to stronger summer precipitation changes over the Alpine region, using climate change projections with a regional atmospheric model of ~12-km grid. VHR uses a similar resolution but on a global scale, without the need to be constrained by lower resolution models.

34

On the negative side, we find that increased model resolution alone can be insufficient to reduce important and well-known biases in the climate or even cause model degradation in VHR. The warm bias over the coastal tropical upwelling areas, the Southern Ocean warm bias, and the rainfall excess bias over warm tropical waters all persist or even increase in VHR compared to HR and LR. These biases point to deficiencies in the model physics, specially in the atmosphere, and more particularly, in the cloud parameterizations. In VHR, both the warm bias over eastern tropical upwelling areas and the Southern Ocean are connected to negative biases in cloud cover. This reinforces the established idea that insufficient stratocumulus decks over the upwelling areas (e.g., Richter, 2015) and mixed-phase clouds over the Southern Ocean (e.g., Hyder et al., 2018) play key roles in setting up those bias. Cloud biases can be particularly insensitive to increases in model resolution, both in the ocean and atmosphere, from ~100-km grids to 25–50-km grids (Moreno-Chamarro et al., 2022). Yet, for example, improved cloud microphysics closer to observations have been shown to help reduce shortwave radiation biases over the Southern Ocean in the Met Office's Unified Model (Varma et al., 2020). Reducing these biases as much as possible is critical, since they can have wider, global impacts on the climate, driving, for example, additional biases in tropical precipitation through the effect on the global energy budget (e.g., Hwang et al., 2013; Hawcroft et al., 2017).

It is interesting to note, nonetheless, that although LR, HR, and VHR all share the same cloud scheme, it is VHR that develops the strongest Southern Ocean bias. This might be related to the lack of additional model tuning from LR to HR and VHR. Rackow et al. (2024) showed that tuning the top-of-the-atmosphere radiation contributed to reducing the warming excess over the Southern Ocean in the IFS-FESOM global model at ~5-km resolution. The HighResMIP protocol suggests that no tuning is performed across resolutions to ensure any changes in the simulated climate can solely be attributed to changes in resolution (Haarsma et al., 2016). This approach can lead to undesired model degradation: for example, the untuned, low-resolution ECMWF model for HighResMIP shows an overly weak AMOC and a large cold bias over the North Atlantic compared to its well-tuned, high-resolution counterpart (Roberts C.D. et al., 2018). This can hinder model comparison and a clean understanding of the effect of model resolution, as biases can have large-scale climatic impacts (e.g., Hwang et al., 2013; Hawcroft et al., 2017; Lee et al., 2018) and affect the response sensitivity to forcing (e.g., McGee et al., 2018).

35

With respect to the spin-up, the HighResMIP protocol suggests a 50-year period (Haarsma et al., 2016). For all the configurations, this period is insufficient to equilibrate the full ocean, although the upper 10~~0~~0 m equilibrates faster than the lower-part, and VHR does it faster and appears more stable after 100 years than HR and LR. The eddy-rich HadGEM3-GC3.1 also shows smaller drifts at the end of the 50-year period than its lowest resolution versions (Roberts et al., 2019). By contrast, for the CESM1.3 model, the low and high-resolution configurations only show a more stable climate after 150 years, related to a strong top-of-the-atmosphere energy imbalance (Chang et al., 2020). This led the authors to propose “150 to 200 years of model spin-up as a future strategy for initializing HR climate model simulations” (Chang et al., 2020). However, considering how computationally expensive these simulations are, new techniques might need to be introduced to tune and spin these models up faster and for longer. As much as tuning can still be “artisanal in character” at many research centers (Mauritsen et al., 2012), new and faster methods are being implemented to speed up the exploration of the space of parameters to find the best fit with observations. These methods include for example machine learning (Hourdin et al., 2021), simplified configurations (Wan et al., 2014) , adjoints (Lyu et al., 2018), or model emulators (Williamson et al., 2013). Additional techniques have also been proposed to spin models up faster at much less computational costs; these include using for example Newton-Krylov methods (Bernsen et al., 2008; Merlis and Khatiwala, 2008), or replacing the atmosphere model by model data (Lofverstrom et al., 2020). Implementing similar techniques in future HR and VHR simulations would help accelerate both the spin-up and tuning phases.

To summarize, we here present the eddy-rich version of the EC-Earth global climate model, EC-Earth3P-VHR, with atmospheric and oceanic resolutions of 10–15 km. The analysis of its main climate features reveals improvements with respect to two lower resolution versions, such as a reduced dry equatorial bias over the Pacific, a more realistic Gulf Stream representation, and more accurate rainfall over mountain areas. Other biases persist or degrade, such as the warm biases over the subtropical upwelling regions and Southern Ocean, ~~or~~ the tropical precipitation excess, or the excess in sea ice volume and oceanic deep mixing in the Arctic. VHR's global resolution is at a similar level of many regional models, such as those participating in CORDEX, and it is much finer than most of the standard CMIP models. This opens a window of opportunity for model comparison and evaluation, as well as process understanding of much more realistic present-day and future climate and on a more regional scale.

36

Code and Data Availability

The data of the EC-Earth3P-LR and -HR models are available from ESGF (https://esgf-index1.ceda.ac.uk/search/cmip6-ceda/, last access: 20 June 2024) via the references provided in Section 2.3: EC-Earth3P (https://doi.org/10.22033/ESGF/CMIP6.4683, EC-Earth, 2018; https://doi.org/10.22033/ESGF/CMIP6.4682, EC-Earth, 2019). Data of ERA-5 are freely available at https://www.ecmwf.int/en/forecasts/dataset/ecmwf-reanalysis-v5 (Hersbach et al., 2020; https://doi.org/10.24381/cds.6860a573, Hersbach et al., 2019), while GPCP data are at https://psl.noaa.gov/data/gridded/data.gpcp.html (Adler et al., 2003), ESA cloud cover data are at https://climate.esa.int/en/projects/cloud/data/ (Stengel et al., 2020), EN4 data version 4.2.2 are at https://www.metoffice.gov.uk/hadobs/en4/ (Good et al., 2013), OSI SAF (OSI-409/OSI-409-a) sea ice concentration data are at https://osi-saf.eumetsat.int/products/sea-ice-products (EUMETSAT Ocean and Sea Ice Satellite Application Facility, 2015), GIOMAS sea ice volume data are at https://psc.apl.washington.edu/zhang/Global_seaice/data.html (Zhang and Rothrock, 2003), and J-OFURO3 flux data are at https://www.j-ofuro.com/en/dataset/ (Tomita et al., 2019). The model data and plot scripts to reproduce the figures can be obtained from https://zenodo.org/records/12078052 (Moreno-Chamarro, 2024). The model code developed at ECMWF, including IFS and the Finite Volume Module (FVM), is intellectual property of ECMWF and its member states. Permission to access the EC-Earth source code can be requested from the EC-Earth community via the EC-Earth website (http://www.ec-earth.org/, last access: July 2024) and may be granted, if a corresponding software license agreement is signed with ECMWF. The repository tag for the version of IFS and EC-Earth3P-VHR used in this work is 3.2.2 (see Section 2.1) and is available through r8643. The EC-Earth workflow software used to run the simulations at the BSC, Auto-EC-Earth, is stored and version controlled in the BSC Earth Sciences GitLab repository (https://earth.bsc.es/gitlab/es/auto-ecearth3, last access: July 2024). Permission to access the repository can be requested from the Earth Sciences Department at the BSC and may be granted, if the applicant has access to the EC-Earth code and the BSC HPC infrastructure. The workflow management system for running the simulations is distributed under Apache License 2.0 as a public project (https://earth.bsc.es/gitlab/es/autosubmit, last access: July 2024) in the BSC GitLab repository.

37

Author Contributions

TA, MA, MC, EF, and SP developed the model setup. EMC and TA ran the simulations. PAB and DK post-processed and cmorized the model data. EMC analyzed the data and wrote the manuscript with input from all the authors.

Competing interests

The authors declare that they have no conflict of interest.

Acknowledgements

This research has been supported by the Horizon2020 PRIMAVERA project (H2020 GA 641727). EMC acknowledges funding from the Spanish Science and Innovation Ministry (Ministerio de Ciencia e Innovación) via the STREAM project (PID2020-114746GB-I00). MA has received funding from the National Research Agency through OEMES (PID2020-116324RA-I00). This work has received funding from the European High Performance Computing Joint Undertaking (JU) under the ESiWACE CoE, grant agreement No 101093054.

References

Abdalla, S., Isaksen, L., Janssen, P. A. E. M., and Nils, W.: Effective spectral resolution of ECMWF atmospheric forecast models, ECMWF Newsletter No. 137, 19–22, https://doi.org/10.21957/rue4o7ac, 2013.

Acosta, M.C., Palomas, S. and Tourigny, E.: Balancing EC-Earth3 Improving the Performance of EC-Earth CMIP6 Configurations by Minimizing the Coupling Cost. Earth and Space Science, 10(8), p.e2023EA002912, https://doi.org/10.1029/2023EA002912, 2023.

Acosta, M. C., Palomas, S., Paronuzzi Ticco, S. V., Utrera, G., Biercamp, J., Bretonniere, P.-A., Budich, R., Castrillo, M., Caubel, A., Doblas-Reyes, F., Epicoco, I., Fladrich, U., Joussaume, S., Kumar Gupta, A., Lawrence, B., Le Sager, P., Lister, G., Moine, M.-P., Rioual, J.-C., Valcke, S., Zadeh, N., and Balaji, V.: The computational and energy cost of simulation and storage for climate science: lessons from CMIP6, Geosci. Model Dev., 17, 3081–3098, https://doi.org/10.5194/gmd-17-3081-2024, 2024.

38

Adler, R. F., Huffman, G. J., Chang, A., Ferraro, R., Xie, P. P., Janowiak, J., Rudolf, B., Schneider, U., Curtis, S., Bolvin, D., and Gruber, A.: The version-2 global precipitation climatology project (GPCP) monthly precipitation analysis (1979–present), J. Hydrometeorol., 4, 1147–1167, https://doi.org/10.1175/1525-7541(2003)004<1147:TVGPCP>2.0.CO;2, 2003 (data available at: https://psl.noaa.gov/data/gridded/data.gpcp.html, last access: 30 March 2023).

Amante, C. and Eakins, B.W.: ETOPO1 arc-minute global relief model: procedures, data sources and analysis, 2009.

Baker, A.J., Schiemann, R., Hodges, K.I., Demory, M. E., Mizielinski, M. S., Roberts, M. J., Shaffrey, L. C., Strachan, J. and Vidale, P. L.: Enhanced climate change response of wintertime North Atlantic circulation, cyclonic activity, and precipitation in a 25-km-resolution global atmospheric model. Journal of Climate, 32(22), 7763–7781, https://doi.org/10.1175/JCLI-D-19-0054.1, 2019.

Balsamo, G., Beljaars, A., Scipal, K., Viterbo, P., van den Hurk,B., Hirschi, M., and Betts, A. K.: A revised hydrology for theECMWF model: Verification from field site to terrestrial waterstorage and impact in the Integrated Forecast System, J. Hydrometeorol., 10, 623–643, 2009.

Becker, J.J., Sandwell, D.T., Smith, W.H.F., Braud, J., Binder, B., Depner, J.L., Fabre, D., Factor, J., Ingalls, S., Kim, S.H. and Ladner, R.: Global bathymetry and elevation data at 30 arc seconds resolution: SRTM30_PLUS. Marine Geodesy, 32(4), 355–371, https://doi.org/10.1080/01490410903297766, 2009.

Bellucci, A., Athanasiadis, P. J., Scoccimarro, E., Ruggieri, P., Gualdi, S., Fedele, G., Haarsma, R. J., Garcia-Serrano, J., Castrillo, M., Putrahasan, D., and Sanchez-Gomez, E.: Air-Sea interaction over the Gulf Stream in an ensemble of HighResMIP present climate simulations, Clim. Dynam., 56, 2093–2111, https://doi.org/10.1007/s00382-020-05573-z, 2021.

Bernsen, E., Dijkstra, H.A., Thies, J. and Wubs, F.W.: The application of Jacobian-free Newton–Krylov methods to reduce the spin-up time of ocean general circulation models. Journal of Computational Physics, 229(21), 8167–8179, https://doi.org/10.1016/j.jcp.2010.07.015, 2010.

 39

Biastoch, A., Schwarzkopf, F. U., Getzlaff, K., Rühs, S., Martin, T., Scheinert, M., Schulzki, T., Handmann, P., Hummels, R. and Böning, C. W.: Regional imprints of changes in the Atlantic Meridional Overturning Circulation in the eddy-rich ocean model VIKING20X. Ocean Science, 17(5), 1177–1211, https://doi.org/10.5194/os-17-1177-2021, 2021.

Bishop, S. P., Small, R. J., Bryan, F. O. and Tomas, R. A.: Scale dependence of midlatitude air–sea interaction. Journal of Climate, 30(20), 8207–8221, https://doi.org/10.1175/JCLI-D-17-0159.1, 2017.

Chang, P., Zhang, S., Danabasoglu, G., Yeager, S.G., Fu, H., Wang, H., Castruccio, F.S., Chen, Y., Edwards, J., Fu, D. and Jia, Y.: An unprecedented set of high-resolution earth system simulations for understanding multiscale interactions in climate variability and change. Journal of Advances in Modeling Earth Systems, 12(12), e2020MS002298, https://doi.org/10.1029/2020MS002298, 2020.

Chassignet, E. and Marshall, D.: Gulf Stream separation in numerical ocean models. Geophysical Monograph Series, 177, https://doi.org/10.1029/177GM05, 2008.

Craig, A., Valcke, S., and Coquart, L.: Development and performance of a new version of the OASIS coupler, OASIS3-MCT_3.0, Geosci. Model Dev., 10, 3297–3308, https://doi.org/10.5194/gmd-10-3297-2017, 2017.

Czaja, A., Frankignoul, C., Minobe, S. and Vannière, B.: Simulating the midlatitude atmospheric circulation: what might we gain from high-resolution modeling of air-sea interactions?. Current climate change reports, 5, 390–406, https://doi.org/10.1007/s40641-019-00148-5, 2019.

Doi, T., Vecchi, G. A., Rosati, A. J., and Delworth, T. L.: Biases in the Atlantic ITCZ in seasonal–interannual variations for a coarse-and a high-resolution coupled climate model, J. Climate, 25, 5494–5511, https://doi.org/10.1175/JCLI-D-11-00360.1, 2012.

Döscher, R., Acosta, M., Alessandri, A., Anthoni, P., Arsouze, T., Bergman, T., Bernardello, R., Boussetta, S., Caron, L.-P., Carver, G., Castrillo, M., Catalano, F., Cvijanovic, I., Davini, P., Dekker, E., Doblas-Reyes, F. J., Docquier, D., Echevarria, P., Fladrich, U., Fuentes-Franco, R., Gröger, M., v. Hardenberg, J., Hieronymus, J., Karami, M. P., Keskinen, J.-P., Koenigk, T., Makkonen, R., Massonnet, F., Ménégoz, M., Miller, P. A., Moreno-Chamarro, E., Nieradzik, L., van Noije, T., Nolan, P., O'Donnell, D., Ollinaho, P., van den Oord, G., Ortega, P., Prims, O. T., Ramos, A., Reerink, T., Rousset, C., Ruprich-

Robert, Y., Le Sager, P., Schmith, T., Schrödner, R., Serva, F., Sicardi, V., Sloth Madsen, M., Smith, B., Tian, T., Tourigny, E., Uotila, P., Vancoppenolle, M., Wang, S., Wårlind, D., Willén, U., Wyser, K., Yang, S., Yepes-Arbós, X., and Zhang, Q.: The EC-Earth3 Earth system model for the Coupled Model Intercomparison Project 6, Geosci. Model Dev., 15, 2973–3020, https://doi.org/10.5194/gmd-15-2973-2022, 2022.

EC-Earth Consortium (EC-Earth): EC-Earth-Consortium EC-Earth3P-HR model output prepared for CMIP6 HighResMIP hist-1950, Earth System Grid Federation [data set; last access: 18 May 2023], https://doi.org/10.22033/ESGF/CMIP6.4683, 2018.

EC-Earth Consortium (EC-Earth): EC-Earth-Consortium EC-Earth3P model output prepared for CMIP6 HighResMIP hist-1950, Earth System Grid Federation [data set; last access: 18 May 2023], https://doi.org/10.22033/ESGF/CMIP6.4682, 2019.

EUMETSAT Ocean and Sea Ice Satellite Application Facility: Global sea ice concentration reprocessing dataset 1978–2015 (v1.2), Norwegian and Danish Meteorological Institutes, available at: https://catalogue.ceda.ac.uk/uuid/8bbde1a8a0ce4a86904a3d7b2b917955 (last access: 8 February 2019), 2015.

Frajka-Williams, E., Ansorge, I.J., Baehr, J., Bryden, H.L., Chidichimo, M.P., Cunningham, S.A., Danabasoglu, G., Dong, S., Donohue, K.A., Elipot, S. Heimbach, P., Holliday, N.P., Hummels, R., Jackson, L.C., Karstensen, J., Lankhorst, M., Le Bras, I.A., Lozier, M. S., McDonagh, E.L., Meinen, C.S., Mercier, H., Moat, B.I., Perez, R.C., Piecuch, C.G., Rhein, M., Srokosz, M.A., Trenberth, K.E., Bacon, S., Forget, G., Goni, G., Kieke, D., Koelling, J., Lamont, T., McCarthy, G.D., Mertens, C., Send, U.,Smeed, D.A., Speich, S., van den Berg, M.,Volkov,D., Wilson, C.: Atlantic Meridional Overturning Circulation: Observed Transport and Variability, Frontiers in Marine Science, 6, https://doi.org/10.3389/fmars.2019.00260, 2019.

Giorgi, F., Torma, C., Coppola, E., Ban, N., Schär, C. and Somot, S.: Enhanced summer convective rainfall at Alpine high elevations in response to climate warming. Nature Geoscience, 9(8), 584-589, https://doi.org/10.1038/ngeo2761, 2016.

Good, S. A., M. J. Martin, M. J., and Rayner, N. A.: EN4: quality controlled ocean temperature and salinity profiles and monthly objective analyses with uncertainty estimates, Journal of Geophysical Research: Oceans, 118, 6704-6716, https://doi.org/10.1002/2013JC009067, 2013 (data available at: https://www.metoffice.gov.uk/hadobs/en4/, last access: 12 November 2021).

Gutjahr, O., Jungclaus, J. H., Brüggemann, N., Haak, H. and Marotzke, J.: Air-sea interactions and water mass transformation during a katabatic storm in the irminger sea. Journal of Geophysical Research: Oceans, 127(5), e2021JC018075,https://doi.org/10.1029/2021JC018075, 2022.

Gutjahr, O., Putrasahan, D., Lohmann, K., Jungclaus, J.H., von Storch, J.S., Brüggemann, N., Haak, H. and Stössel, A.: Max Planck Institute earth system model (MPI-ESM1.2) for the high-resolution model intercomparison project (HighResMIP). Geoscientific Model Development, 12(7), 3241–3281, https://doi.org/10.5194/gmd-12-3241-2019, 2019.

Haarsma, R., Acosta, M., Bakhshi, R., Bretonnière, P. A., Caron, L. P., Castrillo, M., Corti, S., Davini, P., Exarchou, E., Fabiano, F. and Fladrich, U.: HighResMIP versions of EC-Earth: EC-Earth3P and EC-Earth3P-HR–description, model computational performance and basic validation. Geoscientific Model Development, 13(8), 3507–3527, https://doi.org/10.5194/gmd-13-3507-2020, 2020.

Haarsma, R. J., Roberts, M. J., Vidale, P. L., Senior, C. A., Bellucci, A., Bao, Q., Chang, P., Corti, S., Fučkar, N. S., Guemas, V., von Hardenberg, J., Hazeleger, W., Kodama, C., Koenigk, T., Leung, L. R., Lu, J., Luo, J.-J., Mao, J., Mizielinski, M. S., Mizuta, R., Nobre, P., Satoh, M., Scoccimarro, E., Semmler, T., Small, J., and von Storch, J.-S.: High Resolution Model Intercomparison Project (HighResMIP v1.0) for CMIP6, Geosci. Model Dev., 9, 4185–4208, https://doi.org/10.5194/gmd-9-4185-2016, 2016.

Haarsma, R., Acosta, M., Bakhshi, R., Bretonnière, P.-A., Caron, L.-P., Castrillo, M., Corti, S., Davini, P., Exarchou, E., Fabiano, F., Fladrich, U., Fuentes Franco, R., García-Serrano, J., von Hardenberg, J., Koenigk, T., Levine, X., Meccia, V. L., van Noije, T., van den Oord, G., Palmeiro, F. M., Rodrigo, M., Ruprich-Robert, Y., Le Sager, P., Tourigny, E., Wang, S., van Weele, M., and Wyser, K.: HighResMIP versions of EC-Earth: EC-Earth3P and EC-Earth3P-HR – description, model computational performance and basic validation, Geosci. Model Dev., 13, 3507–3527, https://doi.org/10.5194/gmd-13-3507-2020, 2020.

Hawcroft, M., Haywood, J.M., Collins, M., Jones, A., Jones, A.C. and Stephens, G., 2017. Southern Ocean albedo, inter-hemispheric energy transports and the double ITCZ: Global impacts of biases in a coupled model. Climate Dynamics, 48, 2279–2295, https://doi.org/10.1007/s00382-016-3205-5, 2017.

Hazeleger, W., Wang, X., Severijns, C., Ştefănescu, S., Bintanja, R., Sterl, A., Wyser, K., Semmler, T., Yang, S., van den Hurk, B., van Noije, T., van der Linden, E., and van der Wiel, K.: EC-Earth V2.2: description and validation of a new seamless earth system prediction model, Clim. Dynam., 39, 2611–2629, 2012.

Hewitt, H. T., Bell, M. J., Chassignet, E. P., Czaja, A., Ferreira, D., Griffies, S. M., Hyder, P., McClean, J. L., New, A. L., and Roberts, M. J.: Will high-resolution global ocean models benefit coupled predictions on short-range to climate timescales?, Ocean Model., 120, 120–136, https://doi.org/10.1016/j.ocemod.2017.11.002, 2017.

Hersbach, H., Bell, B., Berrisford, P., Biavati, G., Horányi, A., Muñoz Sabater, J., Nicolas, J., Peubey, C., Radu, R., Rozum, I., Schepers, D., Simmons, A., Soci, C., Dee, D., and Thépaut, J.-N.: ERA5 monthly averaged data on pressure levels from 1979 to present, Copernicus Climate Change Service (C3S) Climate Data Store (CDS) [data set], https://doi.org/10.24381/cds.6860a573, 2019.

Hersbach, H., Bell, B., Berrisford, P., Hirahara, S., Horányi, A., Muñoz-Sabater, J., Nicolas, J., Peubey, C., Radu, R., Schepers, D., Simmons, A., Soci, C., Abdalla, S., Abellan, X., Balsamo, G., Bechtold, P., Biavati, G., Bidlot, J., Bonavita, M., Chiara, G. D., Dahlgren, P., Dee, D., Diamantakis, M., Dragani, R., Flemming, J., Forbes, R., Fuentes, M., Geer, A., Haimberger, L., Healy, S., Hogan, R. J., Hólm, E., Janisková, M., Keeley, S., Laloyaux, P., Lopez, P., Lupu, C., Radnoti, G., de Rosnay, P., Rozum, I., Vamborg, F., Villaume, S., and Thépaut, J.: The ERA5 global reanalysis, Q. J. Roy. Meteor. Soc., 146, 1999–2049, https://doi.org/10.1002/qj.3803, 2020 (data available at: https://www.ecmwf.int/en/forecasts/dataset/ecmwf-reanalysis-v5, last access: 23 January 2020).

Hodges, K. I., Lee, R. W., and Bengtsson, L.: A comparison of extratropical cyclones in recent reanalyses ERA-Interim, NASA MERRA, NCEP CFSR, and JRA-25, J. Climate, 24, 4888–4906, https://doi.org/10.1175/2011JCLI4097.1, 2011.

Hoffmann, J., Bauer, P., Sandu, I., Wedi, N., Geenen, T. and Thiemert, D.: Destination Earth– A digital twin in support of climate services. Climate Services, 30, 100394, https://doi.org/10.1016/j.cliser.2023.100394, 2023.

Hohenegger, C., Korn, P., Linardakis, L., Redler, R., Schnur, R., Adamidis, P., Bao, J., Bastin, S., Behravesh, M., Bergemann, M., Biercamp, J., Bockelmann, H., Brokopf, R., Brüggemann, N., Casaroli, L., Chegini, F., Datseris, G., Esch, M., George, G., Giorgetta, M., Gutjahr, O., Haak, H., Hanke, M., Ilyina, T., Jahns, T., Jungclaus, J., Kern, M., Klocke, D., Kluft, L., Kölling, T., Kornblueh, L., Kosukhin, S., Kroll, C., Lee, J., Mauritsen, T., Mehlmann, C., Mieslinger, T., Naumann, A. K., Paccini, L., Peinado, A., Praturi, D. S., Putrasahan, D., Rast, S., Riddick, T., Roeber, N., Schmidt, H., Schulzweida, U., Schütte, F., Segura, H., Shevchenko, R., Singh, V., Specht, M., Stephan, C. C., von Storch, J.-S., Vogel, R., Wengel, C., Winkler, M., Ziemen, F., Marotzke, J., and Stevens, B.: ICON-Sapphire: simulating the components of the Earth system and their interactions at kilometer and subkilometer scales, Geosci. Model Dev., 16, 779–811, https://doi.org/10.5194/gmd-16-779-2023, 2023.

~~Hohenegger, C., Korn, P., Linardakis, L., Redler, R., Schnur, R., Adamidis, P., Bao, J., Bastin, S., Behravesh, M., Bergemann, M. and Biercamp, J.: ICON-Sapphire: simulating the components of the Earth system and their interactions at kilometer and subkilometer scales. Geoscientific Model Development Discussions, 1–42, https://doi.org/10.5194/gmd-16-779-2023, 2022~~.

Hourdin, F., Williamson, D., Rio, C., Couvreux, F., Roehrig, R., Villefranque, N., Musat, I., Fairhead, L., Diallo, F. B. and Volodina, V.: Process-based climate model development harnessing machine learning: II. Model calibration from single column to global. Journal of Advances in Modeling Earth Systems, 13(6), e2020MS002225, https://doi.org/10.1029/2020MS002225, 2021.

Hwang, Y. T. and Frierson, D. M.: Link between the double-Intertropical Convergence Zone problem and cloud biases over the Southern Ocean, P. Natl. Acad. Sci. USA, 110, 4935–4940, https://doi.org/10.1073/pnas.1213302110, 2013.

Hyder, P., Edwards, J. M., Allan, R. P., Hewitt, H. T., Bracegirdle, T. J., Gregory, J. M., Wood, R. A., Meijers, A. J., Mulcahy, J., Field, P., and Furtado, K.: Critical Southern Ocean climate model biases traced to atmospheric model cloud errors, Nat. Commun., 9, 1–17, https://doi.org/10.1038/s41467-018-05634-2, 2018.

Jacob, D., Petersen, J., Eggert, B., Alias, A., Christensen, O. B., Bouwer, L. M., Braun, A., Colette, A., Déqué, M., Georgievski, G. and Georgopoulou, E.: EURO-CORDEX: new

 44

high-resolution climate change projections for European impact research. Regional Environmental Change, 14, 563–578, https://doi.org/10.1007/s10113-013-0499-2, 2014.

Kirtman, B. P., Bitz, C., Bryan, F., Collins, W., Dennis, J., Hearn, N., Kinter, J. L., Loft, R., Rousset, C., Siqueira, L., and Stan, C.: Impact of ocean model resolution on CCSM climate simulations, Clim. Dynam., 39, 1303–1328, https://doi.org/10.1007/s00382-012-1500-3, 2012.

Kriegler, E., Bauer, N., Popp, A., Humpenöder, F., Leimbach, M., Strefler, J., Baumstark, L., Bodirsky, B.L., Hilaire, J., Klein, D., and Mouratiadou, I.: Fossil-fueled development (SSP5): An energy and resource intensive scenario for the 21st century. Global Environmental Change, 42, 297–315, https://doi.org/10.1016/j.gloenvcha.2016.05.015, 2017.

Lee, R.W., Woollings, T. J., Hoskins, B. J., Williams, K. D., O'Reilly, C. H. and Masato, G.: Impact of Gulf Stream SST biases on the global atmospheric circulation. Climate Dynamics, 51, 3369–3387, https://doi.org/10.1007/s00382-018-4083-9, 2018.

Lofverstrom, M., Fyke, J. G., Thayer-Calder, K., Muntjewerf, L., Vizcaino, M., Sacks, W. J., Lipscomb, W. H., Otto-Bliesner, B. L. and Bradley, S. L.: An efficient ice sheet/Earth system model spin-up procedure for CESM2-CISM2: Description, evaluation, and broader applicability. Journal of Advances in Modeling Earth Systems, 12(8), e2019MS001984, https://doi.org/10.1029/2019MS001984, 2020.

Lyu, G., Köhl, A., Matei, I. and Stammer, D.: Adjoint-based climate model tuning: Application to the planet simulator. Journal of Advances in Modeling Earth Systems, 10(1), 207–222, https://doi.org/10.1002/2017MS001194, 2018.

Ma, X., Chang, P., Saravanan, R., Montuoro, R., Nakamura, H., Wu, D., Lin, X. and Wu, L.: Importance of resolving Kuroshio front and eddy influence in simulating the North Pacific storm track. Journal of Climate, 30(5), 1861–1880, https://doi.org/10.1175/JCLI-D-16-0154.1, 2017.

Madec, G.: NEMO reference manual, ocean dynamic component: NEMO-OPA, Note du Pôle modélisation, Inst. Pierre Simon Laplace, France, 2008.

Madec, G. and the NEMO team: NEMO ocean engine version 3.6 stable, Note du Pôle de modélisation de l'Institut Pierre-Simon Laplace No. 27, ISSN: 1288–1619, 2016.

Manubens-Gil, D., Vegas-Regidor, J., Prodhomme, C., Mula-Valls, O. and Doblas-Reyes, F. J.: Seamless management of ensemble climate prediction experiments on HPC platforms. In 2016 International Conference on High Performance Computing & Simulation (HPCS), 895–900, 2016, https://doi.org/10.1109/HPCSim.2016.7568429, 2016.

Mauritsen, T., Stevens, B., Roeckner, E., Crueger, T., Esch, M., Giorgetta, M., Haak, H., Jungclaus, J., Klocke, D., Matei, D. and Mikolajewicz, U.: Tuning the climate of a global model. Journal of advances in modeling Earth systems, 4(3), https://doi.org/10.1029/2012MS000154, 2012.

McDougall, T. J., Barker, P. M., Holmes, R. M., Pawlowicz, R., Griffies, S. M. and Durack, P. J.: The interpretation of temperature and salinity variables in numerical ocean model output and the calculation of heat fluxes and heat content. Geoscientific Model Development, 14(10), 6445–6466, https://doi.org/10.5194/gmd-14-6445-2021, 2021.

McGee, D., Moreno-Chamarro, E., Marshall, J. and Galbraith, E.D.: Western US lake expansions during Heinrich stadials linked to Pacific Hadley circulation. Science advances, 4(11), p.eaav0118, https://doi.org/10.1126/sciadv.aav0118, 2018.

Meehl, G.A., Yang, D., Arblaster, J.M., Bates, S.C., Rosenbloom, N., Neale, R., Bacmeister, J., Lauritzen, P.H., Bryan, F., Small, J. and Truesdale, J.: Effects of model resolution, physics, and coupling on Southern Hemisphere storm tracks in CESM1. 3. Geophysical Research Letters, 46(21), 12408–12416, https://doi.org/10.1029/2019GL084057, 2019.

Merlis, T. M. and Khatiwala, S.: Fast dynamical spin-up of ocean general circulation models using Newton–Krylov methods. Ocean Modelling, 21(3-4), 97–105, https://doi.org/10.1016/j.ocemod.2007.12.001, 2008.

Milinski, S., Bader, J., Haak, H., Siongco, A. C., and Jungclaus, J. H.: High atmospheric horizontal resolution eliminates the wind-driven coastal warm bias in the southeastern tropical Atlantic: Geophys. Res. Lett., 43, 10455–10462, https://doi.org/10.1002/2016GL070530, 2016.

Monteverde, C., De Sales, F. and Jones, C.: Evaluation of the CMIP6 performance in simulating precipitation in the Amazon River basin. Climate, 10(8), 122, https://doi.org/10.3390/cli10080122, 2022.

Moreno-Chamarro, E.: Data for “The very-high resolution configuration of the EC-Earth global model for HighResMIP”, Zenodo [data set, last access: 10 July 2024], https://doi.org/10.5281/zenodo.12078052, 2024.

Moreno-Chamarro, E., Caron, L. P., Ortega, P., Tomas, S. L. and Roberts, M. J.: Can we trust CMIP5/6 future projections of European winter precipitation?: Environmental Research Letters, 16(5), 054063, https://doi.org/10.1088/1748-9326/abf28a, 2021.

Moreno-Chamarro, E., Caron, L. P., Loosveldt Tomas, S., Vegas-Regidor, J., Gutjahr, O., Moine, M. P., Putrasahan, D., Roberts, C. D., Roberts, M. J., Senan, R. and Terray, L.: Impact of increased resolution on long-standing biases in HighResMIP-PRIMAVERA climate models: Geoscientific Model Development, 15(1), 269–289, https://doi.org/10.5194/gmd-15-269-2022, 2022.

Moreton, S., Ferreira, D., Roberts, M. and Hewitt, H.: Air-Sea Turbulent Heat Flux Feedback Over Mesoscale Eddies. Geophysical Research Letters, 48(20), e2021GL095407, https://doi.org/10.1029/2021GL095407, 2021.

Pawlowicz, R.: Key physical variables in the ocean: temperature, salinity, and density. Nature Education Knowledge, 4(4), 13, ~~https://doi.org/10.1029/2021GL095407,~~ 2013.

Pershing, A.J., Alexander, M.A., Hernandez, C.M., Kerr, L.A., Le Bris, A., Mills, K.E., Nye, J.A., Record, N.R., Scannell, H.A., Scott, J.D. and Sherwood, G.D.: Slow adaptation in the face of rapid warming leads to collapse of the Gulf of Maine cod fishery. Science, 350(6262), 809–812, https://doi.org/10.1126/science.aac9819, 2015.

PRIMAVERA and the European Commission: Grant Agreement number: 641727 – PRocess-based climate sIMulation: AdVances in high resolution modelling and European climate Risk Assessment (PRIMAVERA), Zenodo, https://doi.org/10.5281/zenodo.3874429, 2015.

Rai, S., Hecht, M.W., Maltrud, M.E. and Aluie, H.: Scale-dependent Air-Sea Mechanical Coupling: Resolution Mismatch and Spurious Eddy-Killing, https://doi.org/10.22541/essoar.167525271.13326232/v1, 2023.

Rackow, T., Sein, D. V., Semmler, T., Danilov, S., Koldunov, N. V., Sidorenko, D., Wang, Q., and Jung, T.: Sensitivity of deep ocean biases to horizontal resolution in prototype CMIP6 simulations with AWI-CM1.0, Geosci. Model Dev., 12, 2635–2656, https://doi.org/10.5194/gmd-12-2635-2019, 2019.

Rackow, T., Pedruzo-Bagazgoitia, X., Becker, T., Milinski, S., Sandu, I., Aguridan, R., Bechtold, P., Beyer, S., Bidlot, J., Boussetta, S., Diamantakis, M., Dueben, P., Dutra, E., Forbes, R., Goessling, H. F., Hadade, I., Hegewald, J., Keeley, S., Kluft, L., Koldunov, N., Koldunov, A., Kölling, T., Kousal, J., Mogensen, K., Quintino, T., Polichtchouk, I., Sármány, D., Sidorenko, D., Streffing, J., Sützl, B., Takasuka, D., Tietsche, S., Valentini, M., Vannière, B., Wedi, N., Zampieri, L., and Ziemen, F.: Multi-year simulations at kilometre scale with the Integrated Forecasting System coupled to FESOM2.5/NEMOv3.4, EGUsphere [preprint], https://doi.org/10.5194/egusphere-2024-913, 2024.

Renault, L., Lemarié, F. and Arsouze, T.: On the implementation and consequences of the oceanic currents feedback in ocean–atmosphere coupled models. Ocean Modelling, 141, 101423, https://doi.org/10.1016/j.ocemod.2019.101423, 2019.

Renault, L., Marchesiello, P., & Contreras, M.: Coaction of top and bottom drags in Gulf Stream dynamics. Journal of Geophysical Research: Oceans, 128, e2022JC018939. https://doi. org/10.1029/2022JC018939, 2023.

Richter, I.: Climate model biases in the eastern tropical oceans: Causes, impacts and ways forward, Wires Clim. Change, 6, 345–358, https://doi.org/10.1002/wcc.338, 2015.

Roberts, C. D., Senan, R., Molteni, F., Boussetta, S., Mayer, M., and Keeley, S. P. E.: Climate model configurations of the ECMWF Integrated Forecasting System (ECMWF-IFS cycle 43r1) for HighResMIP, Geosci. Model Dev., 11, 3681–3712, https://doi.org/10.5194/gmd-11-3681-2018, 2018.

Roberts, M. J., Baker, A., Blockley, E. W., Calvert, D., Coward, A., Hewitt, H. T., Jackson, L. C., Kuhlbrodt, T., Mathiot, P., Roberts, C. D. and Schiemann, R.: Description of the resolution hierarchy of the global coupled HadGEM3-GC3. 1 model as used in CMIP6 HighResMIP experiments. Geoscientific Model Development, 12(12), 4999–5028, https://doi.org/10.5194/gmd-12-4999-2019, 2019.

Roberts, M. J., Camp, J., Seddon, J., Vidale, P. L., Hodges, K., Vanniere, B., Mecking, J., Haarsma, R., Bellucci, A., Scoccimarro, E., and Caron, L. P.: Impact of model resolution on tropical cyclone simulation using the HighResMIP–PRIMAVERA multimodel ensemble, J. Climate, 33, 2557–2583, https://doi.org/10.1175/JCLI-D-19-0639.1, 2020a.

Roberts, M. J., Jackson, L. C., Roberts, C. D., Meccia, V., Docquier, D., Koenigk, T., Ortega, P., Moreno-Chamarro, E., Bellucci, A., Coward, A., and Drijfhout, S.: Sensitivity of the

 48

Atlantic meridional overturning circulation to model resolution in CMIP6 HighResMIP simulations and implications for future changes, J. Adv. Model. Earth Sy., 12, e2019MS002014, https://doi.org/10.1029/2019MS002014, 2020b.

Roberts, M. J., Vidale, P. L., Senior, C., Hewitt, H. T., Bates, C., Berthou, S., Chang, P., Christensen, H. M., Danilov, S., Demory, M. E., and Griffies, S. M.: The benefits of global high resolution for climate simulation: process understanding and the enabling of stakeholder decisions at the regional scale, B. Am. Meteorol. Soc., 99, 2341–2359, https://doi.org/10.1175/BAMS-D-15-00320.1, 2018.

Saba, V.S., Griffies, S.M., Anderson, W.G., Winton, M., Alexander, M.A., Delworth, T.L., Hare, J.A., Harrison, M.J., Rosati, A., Vecchi, G.A. and Zhang, R.: Enhanced warming of the Northwest Atlantic Ocean under climate change. Journal of Geophysical Research: Oceans, 121(1), 118–132, https://doi.org/10.1002/2015JC011346, 2016.

Sarmany, D., Valentini, M., Maciel, P., Geier, P., Smart, S., Aguridan, R., Hawkes, J. and Quintino, T.: MultIO: A Framework for Message-Driven Data Routing For Weather and Climate Simulations. Proceedings of the Platform for Advanced Scientific Computing Conference, 1–12, https://doi.org/10.1145/3659914.365993, 2024.

Segura, H., Hohenegger, C., Wengel, C. and Stevens, B.: Learning by doing: Seasonal and diurnal features of tropical precipitation in a global-coupled storm-resolving model. Geophysical Research Letters, 49(24), p.e2022GL101796, https://doi.org/10.1029/2022GL101796, 2022.

Sein, D. V., Koldunov, N. V., Danilov, S., Wang, Q., Sidorenko, D., Fast, I., Rackow, T., Cabos, W. and Jung, T.: Ocean modeling on a mesh with resolution following the local Rossby radius. Journal of Advances in Modeling Earth Systems, 9(7), 2601–2614, https://doi.org/10.1002/2017MS001099, 2017.

Semmler, T., Danilov, S., Gierz, P., Goessling, H. F., Hegewald, J., Hinrichs, C., Koldunov, N., Khosravi, N., Mu, L., Rackow, T. and Sein, D. V.: Simulations for CMIP6 with the AWI climate model AWI-CM-1-1. Journal of Advances in Modeling Earth Systems, 12(9), https://doi.org/10.1029/2019MS002009, 2020.

Small, R.J., Bacmeister, J., Bailey, D., Baker, A., Bishop, S., Bryan, F., Caron, J., Dennis, J., Gent, P., Hsu, H.M. and Jochum, M.: A new synoptic scale resolving global climate simulation using the Community Earth System Model. Journal of Advances in Modeling Earth Systems, 6(4), 1065–1094, https://doi.org/10.1002/2014MS000363, 2014.

Small, R. J., Bryan, F. O., Bishop, S. P., and Tomas, R. A.: Air–sea turbulent heat fluxes in climate models and observational analyses: What drives their variability?. Journal of Climate, 32(8), 2397–2421, https://doi.org/10.1175/JCLI-D-18-0576.1, 2019.

Soufflet, Y., Marchesiello, P., Lemarié, F., Jouanno, J., Capet, X., Debreu, L., and Benshila, R.: On effective resolution in ocean models. Ocean Modelling, 98, 36–50, https://doi.org/10.1016/j.ocemod.2015.12.004, 2016.

Stengel, M., Stapelberg, S., Sus, O., Finkensieper, S., Würzler, B., Philipp, D., Hollmann, R., Poulsen, C., Christensen, M., and McGarragh, G.: Cloud_cci Advanced Very High Resolution Radiometer post meridiem (AVHRR-PM) dataset version 3: 35 year climatology of global cloud and radiation properties, Earth Syst. Sci. Data, 12, 41–60, https://doi.org/10.5194/essd-12-41-2020, 2020 (data available at: https://climate.esa.int/en/projects/cloud/data/, last access: 10 March 2021).

Sun, X. and Wu, R.: Spatial scale dependence of the relationship between turbulent surface heat flux and SST. Climate Dynamics, 58(3), 1127–1145, https://doi.org/10.1007/s00382-021-05957-9, 2022.

Tian, B. and Dong, X.: The double-ITCZ bias in CMIP3, CMIP5, and CMIP6 models based on annual mean precipitation, Geophys. Res. Lett., 47, e2020GL087232, https://doi.org/10.1029/2020GL087232, 2020.

Tintó, O., Acosta, M., Castrillo, M., Cortés, A., Sanchez, A., Serradell, K., and Doblas-Reyes, F. J.: Optimizing domain decomposition in an ocean model: the case of NEMO, Procedia Comput. Sci., 108, 776–785, 2017.

Tintó-Prims, O., M. C. Acosta, A. M. Moore, M. Castrillo, K. Serradell, A. Cortés and F. J. Doblas-Reyes: How to use mixed precision in ocean models: exploring a potential reduction of numerical precision in NEMO 4.0 and ROMS 3.6. Geoscientific Model Development, 12, 3135-3148, https://doi.org/10.5194/gmd-12-3135-2019, 2019a.

Tintó, Prims O., M. Castrillo, M. C. Acosta, O. Mula-Valls, A. Sanchez Lorente, K. Serradell, A. Cortés and F. J. Doblas-Reyes: Finding, analysing and solving MPI communication bottlenecks in Earth System models. Journal of Computational Sciences, 36, 100864, https://doi.org/10.1016/j.jocs.2018.04.015, 2019b.

50

Todd, R. E. and Ren, A. S.: Warming and lateral shift of the Gulf Stream from in situ observations since 2001. Nature Climate Change, 13(12), 1348–1352, https://doi.org/10.1038/s41558-023-01835-w, 2023.

Tomita, H., Hihara, T., Kako, S.I., Kubota, M. and Kutsuwada, K.: An introduction to J-OFURO3, a third-generation Japanese ocean flux data set using remote-sensing observations. Journal of Oceanography, 75(2), 171–194, https://doi.org/10.1007/s10872-018-0493-x, 2019 (data available at: https://www.j-ofuro.com/en/dataset/, last access: 14 March 2024).

Tsartsali, E. E., Haarsma, R. J., Athanasiadis, P. J., Bellucci, A., de Vries, H., Drijfhout, S., de Vries, I. E., Putrahasan, D., Roberts, M. J., Sanchez–Gomez, E. and Roberts, C. D.: Impact of resolution on the atmosphere–ocean coupling along the Gulf Stream in global high resolution models. Climate Dynamics, 58(11–12), 3317–3333, https://doi.org/10.1007/s00382-021-06098-9, 2022.

Valcke, S. and Morel, T.: OASIS and PALM, the CERFACS couplers, Tech. rep., CERFACS, 2006.

Váňa, F., Düben, P., Lang, S., Palmer, T., Leutbecher, M., Salmond, D. and Carver, G.: Single precision in weather forecasting models: An evaluation with the IFS. Monthly Weather Review, 145(2), 495–502, https://doi.org/10.1175/MWR-D-16-0228.1, 2017.

Vancoppenolle, M., Bouillon, S., Fichefet, T., Goosse, H., Lecomte, O., Morales Maqueda, M. A., and Madec, G.: The Louvain-la-Neuve sea ice model, Notes du pole de modélisation, Institut Pierre-Simon Laplace (IPSL), Paris, France, No. 31, 2012.

Varma, V., Morgenstern, O., Field, P., Furtado, K., Williams, J., and Hyder, P.: Improving the Southern Ocean cloud albedo biases in a general circulation model, Atmos. Chem. Phys., 20, 7741–7751, https://doi.org/10.5194/acp-20-7741-2020, 2020.

Vidale, P. L., Hodges, K., Vannière, B., Davini, P., Roberts, M. J., Strommen, K., Weisheimer, A., Plesca, E., and Corti, S.: Impact of stochastic physics and model resolution on the simulation of Tropical Cyclones in climate GCMs, J. Climate, 34, 4315–4341, https://doi.org/10.1175/JCLI-D-20-0507.1, 2021.

Wan, H., Rasch, P. J., Zhang, K., Qian, Y., Yan, H. and Zhao, C.: Short ensembles: An efficient method for discerning climate-relevant sensitivities in atmospheric general circulation models. Geoscientific Model Development, 7(5), 1961–1977, https://doi.org/10.5194/gmd-7-1961-2014, 2014.

Wengel, C., Lee, S. S., Stuecker, M. F., Timmermann, A., Chu, J. E., and Schloesser, F.: Future high-resolution El Niño/Southern Oscillation dynamics, Nat. Clim. Change, 1–8, https://doi.org/10.1038/s41558-021-01132-4, 2021.

Williamson, D., Goldstein, M., Allison, L., Blaker, A., Challenor, P., Jackson, L. and Yamazaki, K.: History matching for exploring and reducing climate model parameter space using observations and a large perturbed physics ensemble. Climate Dynamics, 41, 1703–1729, https://doi.org/10.1007/s00382-013-1896-4, 2013.

Woollings, T., Hoskins, B., Blackburn, M., Hassell, D. and Hodges, K.: Storm track sensitivity to sea surface temperature resolution in a regional atmosphere model. Climate Dynamics, 35, 341–353, https://doi.org/10.1007/s00382-009-0554-3, 2010.

Xepes-Arbós, X., G. van den Oord, M. C. Acosta and G. D. Carver: Evaluation and optimisation of the I/O scalability for the next generation of Earth system models: IFS CY43R3 and XIOS 2.0 integration as a case study. Geoscientific Model Development, 15, 379–394, https://doi.org/10.5194/gmd-15-379-2022, 2022.

Zhang, J. and Rothrock, D. A.: Modeling global sea ice with a thickness and enthalpy distribution model in generalized curvilinear coordinates, Mon. Weather Rev., 131, 845–861, https://doi.org/10.1175/1520-0493(2003)131<0845:Mgsiwa>2.0.Co;2, 2003 (data available at: https://psc.apl.washington.edu/zhang/Global_seaice/model.html, last access: 6 March 2019).

Zhang, W., Villarini, G., Scoccimarro, E., Roberts, M., Vidale, P. L., Vanniere, B., Caron, L. P., Putrasahan, D., Roberts, C., Senan, R., and Moine, M. P.: Tropical cyclone precipitation in the HighResMIP atmosphere-only experiments of the PRIMAVERA Project, Clim. Dynam., 57, 253–273, https://doi.org/10.1007/s00382-021-05707-x, 2021.

 52